



HAL
open science

Enhancement and control of laser wakefields via a backward Raman amplifier

J. Ludwig, P.-E. Masson-Laborde, S. Hüller, W. Rozmus, S. Wilks

► **To cite this version:**

J. Ludwig, P.-E. Masson-Laborde, S. Hüller, W. Rozmus, S. Wilks. Enhancement and control of laser wakefields via a backward Raman amplifier. *Physics of Plasmas*, 2018, 25 (5), pp.053108. 10.1063/1.5023387. hal-04449762

HAL Id: hal-04449762

<https://cnrs.hal.science/hal-04449762>

Submitted on 10 Feb 2024

HAL is a multi-disciplinary open access archive for the deposit and dissemination of scientific research documents, whether they are published or not. The documents may come from teaching and research institutions in France or abroad, or from public or private research centers.

L'archive ouverte pluridisciplinaire **HAL**, est destinée au dépôt et à la diffusion de documents scientifiques de niveau recherche, publiés ou non, émanant des établissements d'enseignement et de recherche français ou étrangers, des laboratoires publics ou privés.

Enhancement and Control of Laser Wakefields via a Backward Raman Amplifier

J. D. Ludwig,¹ P-E. Masson-Laborde,² S. Hüller,³ W. Rozmus,¹ and S. C. Wilks⁴

¹⁾*Theoretical Physics Institute, University of Alberta, Edmonton T6G 2E1, Alberta, Canada*

²⁾*CEA, DAM, DIF, F-91297 Arpajon Cedex, France.*

³⁾*Centre de Physique Théorique, CNRS, Ecole Polytechnique, U. Paris-Saclay, 91128 Palaiseau Cedex, France*

⁴⁾*Lawrence Livermore National Laboratory, 7000 East Avenue, Livermore, California 94550, USA*

(Dated: 23 April 2018)

The Backward Raman Amplifier (BRA) is proposed as a possible scheme for improving laser driven plasma wakefields. One- and two-dimensional particle-in-cell code simulations and a 3-Wave coupling model are presented and compared to demonstrate how the BRA can be applied to the laser wakefield accelerator (LWFA) in the non-relativistic regime to counteract limitations such as pump depletion and diffraction. This article provides a discussion on optimal parameters for the combination of BRA and LWFA and a prescription for a BRA pump frequency chirp to ensure coupling beyond the particle dephasing limit. Simulation results demonstrate a reduction or alleviation of the effects of diffraction, an increase in wake amplitude and sustainability, and provide direct insight into new methods of controlling plasma wakes in LWFA and other applications.

PACS numbers: Valid PACS appear here

Keywords: Raman Amplification, Laser Wakefield Acceleration, Particle-In-Cell

I. INTRODUCTION

The ability to create large amplitude plasma waves traveling near the speed of light using a laser pulse has led to several scientific breakthroughs such as laser wakefield acceleration (LWFA)¹, betatron x-ray sources²⁻⁴, and terahertz generation⁵. In general the amplitude and application of these plasma waves can be limited by laser diffraction, depletion, and particle dephasing in the LWFA. In the strongly nonlinear, blow-out regime of the LWFA, dephasing of the relativistic electrons from the accelerating fields, the small charge of the accelerated bunch, and inability to accelerate positive charge for uses such as electron-positron colliders are limitations of this blow-out regime. Several different approaches have been proposed to overcome these drawbacks such as combining the blow-out and the direct laser acceleration scheme⁶. Staged LWFA accelerators⁷ involve a pre-accelerated electron beam from the plasma "bubble" and a long wake field wave in the second acceleration stage. The alternative scenarios of LWFAs usually involve several laser beams and often employ linear wakes over a long acceleration length⁸. Inevitably they result in an increase in the particle beam emittance and come at a cost of increased size and complexity of the accelerator.

In this article we propose another approach, using a Backward Raman Amplifier (BRA) to maintain the driving laser pulse and hence to enhance and control the wakefield generation. Backward Raman amplification and compression⁹⁻¹¹ has been proposed as a laser amplification scheme; it has, however, seen mixed success in experimental demonstrations¹²⁻¹⁴. The experimental efficiency of the BRA scheme is reported to be less than 10%, which is below various theoretical predictions¹⁵. Clearly theoretical understanding of the BRA and of related physical processes remains incomplete. The role of wakefield generation that is emphasized in our paper is one of these physical processes that have not been discussed before in the context of the BRA. This in spite of the fact that wake generation is an inevitable feature of short pulse propagation in a plasma, which as we will demonstrate,

Case	1	2	3	4	5	6
Density n_e/n_c	0.0035	0.015	0.05	0.0035	0.0035	0.0035
T_e [eV]	100	100	50	100	100	100
f-number	30	30	40	15	13	10
Z_R [μm]	3204	3462	7193	801	602	356
t_{pulse} [fs]	30	30	100	30	30	30
$\lambda_p/2c$ [fs]	30	14.5	8	30	30	30
γ_0/ω_{pe}	0.016	0.0126	0.009	0.016	0.016	0.016
a_0	0.0091	0.0091	0.011	0.0091	0.0091	0.0091
a_1	0.205	0.205	0.011	0.205	0.205	0.205

TABLE I. List of all simulations cases.

causes a frequency shift of the seed pulse, and thus affects the BRA coupling. While the overall goal for BRA up to now has been to maximize laser pulse amplification, we consider its use as a control mechanism during plasma wake generation. Specifically, we examine the first application of BRA to amplify and sustain a short seed laser pulse while simultaneously enhancing wakefield generation in a plasma. This article will review short pulse propagation in the context of LWFA (Section II A), followed by a theoretical model for the BRA (Section II B), and present the results of combining the two (Section III A). We will describe the wake’s effects on the BRA (Section III B) and use a chirped pump in the BRA scheme in order to enhance the wakefield generation (Section III C). Finally, our results are summarized in the conclusion (Section IV).

II. INTRODUCTION OF METHODS AND BASIC PROCESSES

The two processes, wake generation and BRA, have been extensively studied on their own. Before examining their nonlinear coupling and interactions we will first review the relevant properties of the linear wake and the backward Raman amplifier. The summary of known results presented below will be useful in further developments of the BRA for the wake field enhancement scenario.

The primary simulation tool in our studies is the relativistic particle-in-cell (PIC) code SCPIC¹⁶ which has been written on the basis of the code Mandor¹⁷ and has already been used in many high intensity laser-plasma applications for electron acceleration and LWFA^{18–21}. As in similar studies^{22–24}, we employ a moving window with the speed of light c . Simulations presented in this article will be labeled with a case number, corresponding to the seed parameters listed in Table I. In all BRA cases the plane wave pump intensity is $1 \times 10^{14} \text{W/cm}^2$, and the wave length is $1.064 \mu\text{m}$. In addition to PIC simulations we will consider a reduced description of the BRA based on a three wave coupling model. The wave coupling equations provide a useful description of the BRA that can be apply to long time and large distances of laser pump and seed interactions in cases where the multidimensional effects, related for example to laser pulse diffraction, are not dominant.

A. Wake Generation

The focus of our work is on short nonrelativistic pulses with a pulse duration, t_{pulse} (FWHM), comparable in spatial extent to the plasma wavelength $ct_{pulse} \sim \lambda_p$ (with $\lambda_p = 2\pi/k_p$, $k_p = \omega_{pe}/c$, where ω_{pe} is the plasma frequency and c is the speed of light). The primary effect of short pulses on the background plasma is wake generation in the form of a longitudinal plasma wave at wave length λ_p and phase velocity $v_p \approx c$. We denote in the following such pulses as “seed” pulses with the field amplitude a_1 . In the linear approximation, the plasma electron density perturbation associated with the wake, δn_w , is

given by¹

$$\frac{\delta n_w}{n_0}(\zeta, y, z) = -\frac{c/v_{g1}}{4k_p} \int_{\zeta}^{\infty} d\zeta' \sin[k'_p(\zeta - \zeta')] \nabla_{\zeta', y, z}^2 |a_1|^2, \quad (1)$$

where $\zeta = x - v_{g1}t$ denotes the coordinate in the frame where the seed pulse moves with the group velocity v_{g1} in x -direction, n_0 denotes the background plasma electron density, and where the seed electric field amplitude is given by $a_1 = \frac{eE_1}{m_e c \omega_1} = 8.55 \times 10^{-10} (I_1 \lambda_1^2 [Wcm^{-2} \mu m^2])^{1/2}$ in terms of the intensity of the short seed laser pulse I_1 and its wavelength λ_1 ($\lambda_1 = 1.13 \mu m$ when $n_e = 0.0035 n_c$, where n_c is the critical electron density for this laser frequency), and $k'_p = \omega_{pe}/v_{g1}$. The operator $\nabla_{\zeta', y, z}^2 = \partial_{\zeta'^2}^2 + \partial_{y^2}^2 + \partial_{z^2}^2$ is taken along the axis. To illustrate the pertinence of this expression, Eq. (1), we compare it in Fig. 1a with results from SCPIC simulations for a seed pulse having initially a Gaussian envelope with full-half-width-maximum (FWHM) of $t_{pulse} = 30$ fs in time (and $l_s = ct_{pulse} \approx 9 \mu m$ in length) and the peak seed pulse of amplitude $a_1 = 0.205$ in a plasma with density $n_e/n_c = 0.0035$ cf. Ref.²⁵. This simulation corresponds to case “1”, see herefore Table I for all simulation cases discussed.

FIG. 1. In the short pulse regime, case “1” (see Table I): (a) 1D cut in x at $y = 0$ of fields and density from 2D PIC and theory, (b) Longitudinal wakefield from PIC, (c) Transverse wakefield from PIC. In the self-modulated regime, case “2”: (d) 1D cut of fields and density from PIC, (e) Longitudinal wakefield from PIC, (f) Transverse component of wakefield from PIC. In both cases the initial seed amplitude is $a_1 = 0.205$, and initial seed duration is 30fs. Plasma densities are respectively $n_e/n_c = 0.0035$ (case “1”) (a)-(c) and $n_e/n_c = 0.015$ (case “2”) (d)-(f), taken at time $t = 1.16$ ps in the short pulse regime, and $t = 13.19$ ps in the self-modulated regime. Both PIC simulations were run with 30 cells/ μm resolution, and 9 particles/cell, the simulation domains were $150 \times 300 \mu m$ for case “1” and $200 \times 200 \mu m$ for case “2”.

The generation of the wake is not a resonant process but Eq. (1) predicts maximum response for $l_s = \lambda_p/2$. Alternatively, longer pulses $l_s > \lambda_p$ give rise to “self-modulated” (SM) solutions where the wake Langmuir wave is generated at the front of the laser pulse and couples resonantly to the seed via forward Raman instability.

The simulation shown in Figures 1d,e,f, corresponding to case “2” (see Table I) illustrates, the regime of a self-modulated seed pulse with a large-amplitude wake. Except for the higher plasma density, $n_e/n_c = 0.015$, resulting in a shorter plasma wave length λ_p , case “2” has the same conditions as case “1”.

FIG. 2. Wake amplitude vs Propagation Distance reconstructed from subsequent moving window frames of 2D PIC simulation case “4”. The laser is focused to the start of the plasma at $x = 100 \mu m$ and propogates from left to right leaving a wake in the plasma. The theoretical spot size of the laser from is overlaid in black lines with a corresponding Rayleigh length $Z_R \approx 800 \mu m$. After propagating $3Z_R$ the wake amplitude is reduced to approximatly 1/4 its initial amplitude.

To obtain sufficiently high intensities for wakefield generation, laser pulses must first undergo optical focusing. As a result of focusing, the spot size radius of the laser in a vacuum evolves as can be described by: $r(x) = r_0 \sqrt{1 + x^2/Z_R^2}$, where $r(x)$ is the radius of the laser spot size that depends on the propagation distance x and on the Rayleigh length Z_R determined by $Z_R = \pi f^2 \lambda$ where f is the mirror’s f-number and λ the laser wave length. The Rayleigh length indicates the distance of laser propagation where the laser spot size is doubled in area, reducing its intensity by a factor of $2/\sqrt{2}/1$ in 3D/2D/1D. Since the amplitude of the wake depends on a_1^2 in Eq. (1), optimum wake generation requires the driving pulse to be focused close to its diffraction limit r_0 over as long a distance as possible. This can be achieved through the use of large f-number optics; however, physical constraints on the focusing distance limit the maximum f-number available in laboratory and

therefore pulse diffraction can be the significant limiting factor in non-relativistic wakefield acceleration.

Although electron acceleration in the wake fields will not be discussed at length, we consider a dephasing time and length as a characteristic physical constraint for the BRA coupling. Depending on the plasma density and laser wave length, particle dephasing can occur when particles are accelerated to velocities higher than the phase velocity of the wake. These particles eventually overshoot the accelerating phase and are decelerated. Particle dephasing places a length constraint on the region of acceleration. For a highly relativistic electron, in a wake of radial extent much greater than λ_p , the linear dephasing length can be calculated using the relative velocity difference between the particle and wake, the particle beam moves at velocity approximately c , while the wake's phase velocity $v_{ph} = c\sqrt{1 - n_e/n_c}$. This results in the dephasing constraint $(c - v_{ph})t_d = \lambda_p/2$. Defining the dephasing length as $L_d = ct_d$, results in $\lambda_p/2 = L_d[1 - (1 - \lambda^2/\lambda_p^2)^{1/2}]$ being $\approx L_d\lambda^2/2\lambda_p^2$ for $n_e/n_c \ll 1$, so that the dephasing length can be approximated as¹, $L_d \approx \lambda_p^3/\lambda^2$. For a given laser wavelength and plasma density the dephasing length is a constant barrier on particle acceleration that is underutilized due to the diffraction of low f-number lasers. To ensure the wakefield is maintained over the extent of the dephasing length we propose the use of a backward Raman amplifier which allows for corrections to be applied to the wake generating laser during its propagation in the plasma.

B. Backward Raman Amplifier

Backward Raman Amplification (BRA) involves the use of a long pump pulse (ω_0, k_0) counterpropagating with respect to the short seed pulse ($\omega_1 = \omega_0 - \omega_{pe}, k_1 = k_p - k_0$). When the two lasers overlap they beat at the plasma frequency, exciting a Langmuir wave ($\omega_L = \omega_{pe}, k_L \approx 2k_0 - k_p$) that resonantly couples to the seed. Energy flows from pump to seed, resulting in amplification and compression of the seed.

BRA is typically modeled in 1D with a set of three coupled equations for the slowly-varying field envelopes of the waves, the pump wave a_0 , the seed a_1 , and the plasma (Langmuir) wave a_L .¹⁰ We will compare in the following the results from PIC simulations of the BRA with solutions of this 3-wave coupling model defined by the following set of equations¹⁰,

$$[\partial_\tau - (|v_{g0}| + v_{g1})\partial_\zeta] a_0 = -\gamma_0 a_L \hat{a}_1, \quad (2)$$

$$\partial_\tau \hat{a}_1 = \gamma_0 a_0 a_L^*, \quad (3)$$

$$[\partial_\tau - v_{g1}\partial_\zeta + \nu] a_L = \gamma_0 a_0 \hat{a}_1^*, \quad (4)$$

where $a_{0,1} \equiv eE_0/(m_e c \omega_{0,1})$ are the normalized amplitudes of the electromagnetic fields $E_{0,1}$ of the pump (0) and the seed (1) wave, with $\hat{a}_1 = (\omega_0/\omega_1)^{1/2} a_1$, and with $(\omega_{0,1}, \vec{k}_{0,1})$ as the corresponding frequencies and wave vectors; $a_L = (\omega_L/\omega_0)^{1/2} eE_L/(m_e c \omega_p)$ denotes the normalized amplitude of the Langmuir wave electric field, E_L , with (ω_L, \vec{k}_L) and the coupling constant reads $\gamma_0 = (k_L c/4)\omega_p/(\omega_L \omega_1)^{1/2}$. The equations are written in the stationary frame of the seed pulse, using the variables $\zeta = x - v_{g1}t$, $\tau = t$, where v_{g0} and v_{g1} are the pump and seed wave group velocities, and where the Langmuir wave group velocity has been neglected. The damping coefficient ν has been added to the Langmuir wave equation (4). Its functional form and magnitude can simply be the linear Landau damping $\nu_L = (\pi\omega_{pe}^3/2k^2)\partial f_M/\partial v|_{v=\omega_L/k}$ evaluated at the Maxwellian distribution function, f_M . On the long time scale ν may be modified due to nonlinear evolution of Langmuir waves that may include electron trapping and wave coupling. Such long time effects do not usually arise during BRA coupling for short seed pulse durations as in the example of Fig. 3.

Figure 3 illustrates the comparison between PIC simulation and the 3-wave coupling model for parameters corresponding to case "3", leading to the π -pulse solution¹⁰ of Stimulated Raman Scattering (SRS). The seed pulse amplitude at time $t = 3.57$ ps, has already experienced amplification with respect to its initial amplitude $a_1 = 0.011$. Amplification

is due to the pump laser – propagating from the right to the left – initially at $a_0 = 0.011$, through coupling with the Langmuir wave. The seed pulse duration t_{pulse} is 100fs at FWHM, the plasma density and electron temperature are $n_e/n_c = 0.05$ and $T_e = 50\text{eV}$, respectively. The example of case “3”, and previous studies based on PIC simulation with similar parameters^{22,24,27}, have been performed in order to validate 3-wave coupling models. Among these studies, Ref.²⁷ dealt with long time self-similar evolution of 3-wave solutions¹⁰ albeit under idealized conditions of cold background plasma.

FIG. 3. Comparison of field amplitudes between PIC simulation (color and broadened lines as a result of enveloping the fields) and 3-wave coupling model (solid black lines): for the seed, line (2) (with amplitudes $\times 1/2$); for the laser pump, line (1); and the Langmuir wave, line (3), at interaction time $t = 3.57\text{ps}$. Amplitudes are normalized to the incoming pump amplitude. The PIC simulation was run with a simulation domain of $400\mu\text{m}$, $135\text{cells}/\mu\text{m}$ resolution, and 1024 particles/cell.

The good agreement between the 3-wave coupling model (2), (3), (4) and PIC simulation shown in Fig. 3 characterizes the initial short time evolution of BRA. As we will discuss below, plasma wake generation and subsequent seed pulse frequency shift, and self-modulation of the relatively long electromagnetic pulse are among nonlinear effects that limit application of a straightforward 3-wave coupling model. Such limitations motivate a need for PIC simulations when the reduced wave coupling models of BRA are derived.

The different modes in k-space are illustrated in Fig. 4 that shows the electric field spectrum with electrostatic components in orange and electromagnetic components in blue. The laser pump mode at k_0 , the wake at $k_p = \omega_{pe}/c$, the seed at $k_1 = k_0 - k_p$, and the Langmuir waves from Raman coupling $k_L \approx 2k_0 - k_p$. The one dimensional Fourier transform is taken in space and is presented as “FFT(E_y)” and “FFT(E_x)” for the Fourier transform of E_y and E_x , respectively into k_x .

FIG. 4. Electric field power spectrum vs wavenumber, showing electrostatic components in orange and electromagnetic components in blue. (1) Wake at the plasma wavenumber $k_p = \omega_{pe}/c$. (2) Seed at k_1 downshifted by k_p from the pump. (3) Pump defined to be k_0 . (4) Langmuir waves from Raman coupling $k_L \approx 2k_0 - k_p$. Simulation parameters correspond to case “2”.

III. BACKWARD RAMAN AMPLIFIER FOR LASER WAKEFIELD GENERATION

In the following section we will demonstrate the control and enhancement of the laser produced wakefield by combining it with the backward Raman amplifier scheme. For this purpose we present the results of simulations where we bring together both effects, BRA and wakefield, in order to optimize and sustain the laser generated wakefield. We first present the results of 2D PIC simulations for the plasma conditions corresponding to the case “1” from the Table I except for the plane wave limit of the seed and the pump pulses. The discussion of these results will introduce important physical processes related to BRA and wake coupling. Next we will consider BRA as the mechanism that overcomes diffraction of the seed pulse and extends wake generation to at least the timescales on the order of the particle dephasing length, Sec. III A. In the Sec. III B we will present results on timescales much greater than the dephasing length and consider the effects of wakefield generation on the resonance coupling of the BRA. We will also revise a theoretical model for both laser wakefield generation and backward Raman amplification and consider chirp of the pump, cf. Sec. III C, as the mechanism mitigating frequency and wavelength dephasing due to the wake generation.

The results below correspond to a 30 fs FWHM driving a seed laser pulse of intensity $5 \times 10^{16}\text{W}/\text{cm}^2$ at best focus and a flat top plane wave pump of intensity $1 \times 10^{14}\text{W}/\text{cm}^2$, in a plasma of density $n_e = 0.0035n_c$. The parameters are chosen such that the seed efficiently excites plasma waves of the wake ($ct_{seed} = \lambda_p/2$) in the non-relativistic regime

($a_1 = 0.205$), and the pump intensity is sufficiently low such that it does not produce backscattered SRS from the particle noise before interaction with the seed pulse. The spatial SRS gain coefficient of a pump wave, $G = L_x \gamma_0^2 |a_0|^2 / |\nu_L v_{g1}|$, requires the length $L_x \approx 70mm$ to reach $G > 1$ values for the parameters of this example. This estimate corresponds to the background electron temperature of 100 eV and the SRS Langmuir wave of the BRA at $k_L \approx 0.46k_D$. Recent work²⁶ has proposed the use of a "flying focus" on the BRA pump to combat parasitic precursors, such a setup could possibly support larger pump intensities, and hence larger amplification of the seed.

While the low electron density of this example is an optimal choice for the wake generation by the 30 fs laser pulse, the electron temperature of 100 eV is consistent with the experimental conditions of gas jet plasmas²⁸. The resulting large ratio $k_L/k_D \approx 0.46$ of the BRA Langmuir wave characterizes the kinetic regime of the SRS^{29,30} and of the Langmuir wave nonlinear evolution³¹. This leads to strong linear Landau damping, $\nu_L \approx 0.14\omega_{pe}$, and in the nonlinear regime, to electron trapping and to trapped particle modulational instability²⁹⁻³¹. However, the nonlinear physics of Langmuir wave evolution – clearly identifiable in simulation results below – becomes important only on time scales longer than the short seed pulse duration, and therefore it has negligible effect on the BRA and the wakefield generation. Consistently, simulations run at different temperatures (50eV, $k_L \approx 0.32k_D$ and 200eV, $k_L \approx 0.65k_D$) show only small variations in the resulting seed and wake amplitudes (see Fig. 9a,b).

FIG. 5. From 2D plane wave PIC simulation with conditions of case "1": (a) snapshot of the longitudinal electric field in the $x - y$ -plane at $t = 8.0ps$ (x : propagation direction; red/blue color corresponds to positive/negative field values, respectively); the superposed black line shows the transverse field of the seed pulse and pump from a cut at $y = L_y/2$; (b) spectrum of the electrostatic field in the $k_x - k_y$ plane with subfigure showing a line-out at $k_y=0$, both at the same time instant as in panel (a); (c) spectrum of electromagnetic field (summed over k_y) as a function of time. The PIC simulation was run with a simulation domain of $10 \times 200 \mu m$, $40 \text{ cells}/\mu m$ resolution, and 16 particles/cell.

Figure 5 shows the results of a 2D plane wave seed and pump simulation with parameters of case "1", the transverse dimension of $10 \mu m$ and the transverse periodic boundary conditions. The three panels in Fig. 5 illustrate the main physical processes involved in the simultaneous BRA and the wakefield generation. Figure 5a displays longitudinal electric field of the Langmuir waves due to SRS at $k_L \approx 0.46k_D$ and the wake at $k_p = \omega_{pe}/c \approx 0.014k_D$. Superimposed is the 1D cut at $y = 5 \mu m$ of the transverse electric field due to the seed and the pump lasers. At the time of Fig. 5, $t = 8ps$, the wake is well developed and extends hundreds of microns behind the seed. We have estimated the bounce frequency of trapped electrons in the SRS driven Langmuir wave. At the maximum amplitude of the Langmuir wave electric field such that $eE_L/mc\omega_L \approx 0.02$ (see Fig. 6) the bounce frequency $\omega_b = (k_L eE_L/m)^{1/2} \approx 9.3 \times 10^{13} 1/s$ and therefore the characteristic trapping time $\tau_b = 2\pi/\omega_b = 67.5fs$ is longer than the time of the seed pulse duration and the BRA coupling. On the other hand the freely propagating (to the left) SRS Langmuir waves experience effects of the trapped particles that result in the transverse modulations of their wavefronts on the longer time scale corresponding to the trapped particle modulational instability²⁹⁻³¹. This is seen on the left of Fig. 5a, far behind the leading seed pulse, and in the two dimensional Fourier transform of the longitudinal fields in Fig. 5b. The two dimensional Fourier transforms are taken in space and are presented as "fft2(E_x)" and "fft(E_y)" for the Fourier transform of E_x and E_y , respectively into k_x and k_y , and k_x respectively, (see figure label). The spectra are calculated over the whole length and width of the simulation window and in addition to the wake ($k_x = k_p = 0.059k_0, k_y \approx 0$) and the SRS Langmuir wave ($k_x = k_L = 1.94k_0, k_y \approx 0$) one can see broad continua of transverse components, resulting from the trapped particle modulational instability²⁹⁻³¹ and the second harmonic of the k_L -wave. The detailed analysis of the spectra about $k_x \approx 2k_0$ has revealed additional components at $k_L \pm nk_p$ and $\omega_L \pm n\omega_p$ (cf. insert in Fig. 5b) that result from the coupling

between strong wakefield wave (k_p, ω_p) and SRS driven Langmuir wave. Such coupling takes time and we have found no evidence that it actually affects the BRA interaction due to short seed pulse duration. These extra spectral components in the Langmuir wave fields can modify damping and contribute to frequency shifts, but again, only on the longer time scale than the Raman amplification process.

The focus of this work is on coupling between two nonlinear processes, wakefield generation and BRA. We will demonstrate that wakefield generation can be extended over large plasma distances due to the BRA enhancing the amplitude of the seed pulse. On the other hand, the presence of several spectral components in the electrostatic fields can lead to deleterious effects such as producing different components at $k_L \pm nk_p$ and $\omega_L \pm n\omega_p$ or adding frequency shifts and instabilities due to trapped particles. These effects influence SRS Langmuir wave on the long time scale. We have also found that the time dependent density modifications due to wake produce k-vector and frequency shifts of the electromagnetic seed pulse. This effect is illustrated in Fig. 5c and will become central to our discussions in the following sections (cf. Fig. 13b). Despite our focus on short seed pulses (that extend half of a plasma wavelength) to maximize wakefield generation, the wake Langmuir waves are always created by high intensity femtosecond laser pulses, and therefore the BRA schemes should verify whether the wake will introduce frequency and wavelength shifts and account for these decoupling effects in the reduced models based on the three wave approximation.

The characteristic feature of the electrostatic field spectra is large separation between the wake at k_p and the SRS Langmuir wave at k_L (cf. spectral components 1 and 4 in Fig. 4 respectively). On the other hand the electromagnetic field components of the seed pulse (marked as 2 in Fig. 4) and of the pump (number 3), can overlap for lower densities than in case “2” (see table) of Fig. 4. This has been the condition of the current case “1” at $n_e/n_c = 0.0035$. Therefore in the comparison between the three wave coupling model, (2), (3), (4) and PIC simulations in Fig. 6 we have plotted the seed and pump wave amplitudes together. Note the remarkable agreement for the Langmuir wave amplitudes near the vicinity of the seed and discrepancy on the longer distance scale due to nonlinear effects including particle trapping and coupling to the wake. The three wave coupling model in Fig. 6 was solved with the Langmuir wave damping coefficient, $\nu = \nu_L = 0.14\omega_p$. In general we have found weak dependence at the early time, i.e. until the first maximum in the Langmuir wave amplitude, on the damping coefficient ν (cf. also Ref.³⁰).

FIG. 6. From 2D plane wave PIC simulation with conditions of case “1”: Comparison of field amplitude between PIC simulation (color and broadened lines as a result of enveloping the fields) and 3-wave coupling model (solid black line): for the pump+seed, line (1); and the Langmuir wave, line (2) (with amplitudes $\times 100$), at interaction time $t = 2.61\text{ps}$. Amplitudes are normalized to the initial seed amplitude. The PIC simulation was run with a simulation domain of $10 \times 200 \mu\text{m}$, $40\text{cells}/\mu\text{m}$ resolution, and 16 particles/cell.

For optimal BRA coupling the seed pulse duration should be long enough such that its spectral bandwidth is localized to the BRA resonance region; however, optimal wake generation requires the seed pulse duration to be of the order of half a plasma wavelength, $ct_{pulse} \sim \lambda_p/2$, and the SRS growth rate increases with plasma density (shorter plasma wavelength). A chirped pump has previously been used to extend coupling in the BRA to all spectral components of a short seed pulse³². The effect of the broad seed pulse spectrum was examined in PIC simulations³³ showing Brillouin coupling³⁴ in the BRA amplification and compression scheme. Since our seed pulses are short and relatively low intensity, Brillouin coupling is expected to be unimportant. Our plasma density and seed pulse length parameters were chosen to be in a demonstrated region of optimal amplification²³, to be experimentally relevant, and to balance the effects of density on BRA coupling.

FIG. 7. Simulation results with $f/15$ at $t=0.776ps$. Laser polarization is in the y-direction and propagation is in the x-direction. (a) E_y with BRA, (b) E_y without BRA, (c) Difference in E_y between the subcases with and without BRA, (d) E_x with BRA, (e) E_x without BRA, (f) Difference in E_x between the subcases with and without BRA. Subplots (c)& (f) are obtained by $\Delta E_{x(y)} = E_{x(y)}(\text{without BRA}) - E_{x(y)}(\text{with BRA})$. Both PIC simulations of case “4” were run with a simulation domain of $150\mu m \times 300\mu m$, $30\text{cells}/\mu m$ resolution, and 9 particles/cell.

A. Resonant BRA

Figure 7 shows the layout of the $f/15$ simulations (case “4”), where the laser propagation is in the x-direction, and polarization is in the y-direction. In Figures 7 we compare the fields resulting from a simulation without BRA, E_x in Fig. 7a and E_y in Fig. 7b, to the simulation with BRA, Figs. 7d and e respectively, for case ”4”. Figures 7c and 7f show the difference in each field component between both cases, namely $\Delta E_{x(y)} = E_{x(y)}(\text{with BRA}) - E_{x(y)}(\text{without BRA})$. From the quantity ΔE_y in Fig.7c, it can be seen that the seed pulse is enhanced as it passes through the plane wave pump (oscillation amplitude $\sim 9 \times 10^{-3}$ outside wake region), leaving a trail of depletion in the plane wave pump. Figure 7f shows enhancement to the wake due to the amplification of the seed.

FIG. 8. Evolution of the energy density of a $f/15$ seed in a plasma vs propagation time and transverse space. a) With no amplifier. b) With a Raman amplifier. The laser is at maximum focus at $t = 0.2ps$. Simulation parameters correspond to those of case “4”.

Figure 8 shows the time evolution of the seed’s energy density with and without BRA. Without BRA the $f/15$ seed quickly diffracts resulting in much lower wake amplitude. With BRA the $f/15$ seed still diffracts, see Fig. 8b, however the energy density is nearly maintained by the BRA allowing the seed to continue to produce a large wake.

FIG. 9. Comparison of seed and wake amplitudes with (red) and without (blue) BRA. (a) Seed amplitude comparison $f/30$, (b) Seed amplitude comparison $f/15$ with theory from Eq. (5) shown by the dashed black line, (c) Seed amplitude comparison SM $f/30$, (d) Wake amplitude comparison $f/30$, (e) Wake amplitude comparison $f/15$, (f) Wake amplitude comparison SM $f/30$. Simulation parameters correspond to those of case “1” for (a) & (d), case “4” for (b) & (e), and case “2” for (c) & (f).

In the $f/30$ case, Figs. 9a and 9d, the amplifier operates faster than the pulse diffraction. This leads to significant enhancement of the pulse and wake until decoupling from the wake induced frequency shift. In the $f/15$ case, Figs. 9b and 9e, the amplifier provides additional energy but at early times the pulse diffracts quicker than it can be replenished. In the $f/15$ case the competition between diffraction and amplification reaches a balance and the wake is maintained at nearly the same or higher amplitude than the unamplified pulse as shown in Fig. 9e. In the higher density plasma of case “2” the seed experiences modulation by its wake (Fig. 1d) which – despite diffraction – results in a focusing that increases the seed amplitude with or without the BRA. When a BRA is applied to case “2” there is improved BRA coupling due to the higher plasma density, this results in a large enhancement to both the seed and wake amplitude as shown in Figs. 9c and 9f.

A simple model that is consistent with PIC simulations is proposed to describe competition between diffraction effects and the BRA. Assuming that the seed pulse is well approximated by the Gaussian solution to the wave equation during the BRA interaction, we can model the intensity evolution of the seed taking into account both the effects of diffraction and the BRA. Typical results of the BRA for the wake generation are illustrated in Figs. 9. Apart from case “3”, all our BRA simulations are in the superradiant regime^{9,35,36} ($\omega_{pe} \leq 2\omega_0\sqrt{a_0a_1}$) where the laser pump is strongly depleted as it transfers energy to the seed. This can be clearly observed in Fig. 7c displaying depleted pump behind the right propagating seed pulse. With the parameter $0 \leq \alpha \leq 1$ being the efficiency of the energy flow from pump to seed, the incremental energy ($d\mathcal{E}$) transfer from pump to seed

during time dt , is $d\mathcal{E}_1 = -d\mathcal{E}_0 = 2\alpha I_0 A_1(t)dt$. Where $A_1(t)$ is the time dependant spot size area of the seed laser, and the factor of 2 arises due to the counterpropagation of the pump and seed. Integrating this results in order to obtain the seed intensity evolution gives

$$I_1(t) = \left[\frac{2\alpha c}{l_s} \int_0^t I_0(t') \left[1 + \left(\frac{ct'}{Z_R} \right)^2 \right]^{\frac{d-1}{2}} dt' + I_1(0) \right] \left[1 + \left(\frac{ct}{Z_R} \right)^2 \right]^{\frac{1-d}{2}}, \quad (5)$$

where d indicates the spatial dimension of the solution, i.e. $d=2$ or $=3$ for 2D or 3D respectively, $l_s = ct_{pulse}$, and Z_R is the Rayleigh length of the seed pulse. The solution to Eq. (5) with $\alpha = 0.45$ efficiency and constant pump intensity $I_0 = 1 \times 10^{14} W/cm^2$ shows good agreement with PIC simulation case “4” in Fig. 9b. We can estimate the energy transfer from the pump to the seed in order to balance intensity loss due to diffraction. To determine the pump intensity constraint one can set $\frac{\partial I_1}{\partial t} = 0$ to get the solution:

$$I_0(t) = I_1(0) \frac{d-1}{2} \frac{l_s}{\alpha Z_R} \left[1 + \left(\frac{ct}{Z_R} \right)^2 \right]^{-1} \frac{ct}{Z_R}, \quad (6)$$

One can verify this result by substituting Eq. (6) into Eq. (5) to confirm $I_1(t) = I_1(0)$. Since diffraction results in a dynamic loss in seed intensity, the pump requirements $I_0(t)$ (6) are not constant in time, but can be evaluated near the seed’s Rayleigh length ($t \approx Z_R/c$, where losses are strongest) to find a constant pump intensity that ensures diffraction is always overcome. As seen in PIC simulation case “4” (c.f. Fig. 9b) Eq. (6) (with $\alpha = 1$) predicts a BRA pump of intensity $3 \times 10^{14} W/cm^2$ while our BRA pump intensity is $1 \times 10^{14} W/cm^2$ hence it is impossible for our pump to overcome diffraction near the Rayleigh length (simulation time, $t \approx 4ps$) but our pump is more than sufficient to maintain the pulse at later times.

FIG. 10. Limiting lengths for particle energy gain (in 2D) as a function of the seed pulse aperture (f-number) for a 30fs driving pulse in a plasma of density $n_e = 0.0035n_c$. LWFA without BRA is restricted to the green region; when a BRA is applied diffraction is overcome allowing access to the yellow region. Markers indicate results from PIC simulations (run until the dephasing time $t \approx 17ps$). The diffraction limit is defined to be the length at which diffraction causes the wake amplitude to be $\leq 75\%$ of its maximum unamplified value. The 3D diffraction limit without BRA is shown by the dashed line; the dephasing length remains constant in 3D.

Figure 10 summarizes the results of 2D PIC simulations of BRA applied to LWFA. Efficient particle acceleration can be limited by diffraction of the pulse, but is ultimately dictated by the particle dephasing length. For a range of experimentally relevant f-numbers, Fig. 10 demonstrates that BRA applied to LWFA can help maintain the wake amplitude of diffracting lasers and allow for better or full use of the particle dephasing limit. Simulation results in our standard parameters (cases “1”, “4”, “5”, “6”) show that when a BRA pump of intensity $I_0 = 1 \times 10^{14} W/cm^2$ is applied to seed lasers with best-focus intensity $I_1(0) = 5 \times 10^{16} W/cm^2$, the effects of diffraction are overcome for f-numbers of 15 or larger, but enhancement cannot continue indefinitely. In the next section we will discuss a new saturation mechanism of the BRA in context to wake generation.

B. Loss of the BRA resonance due to the wake effects

In this section we examine the BRA applied to LWFA at times exceeding particle dephasing. For our standard parameters (cases “1” & “4”) particle dephasing happens at $t \approx 17ps$ ($t \approx 1.5ps$ for SM case “2”), however BRA and LWFA applications that are not concerned about dephasing (ex: betatron x-ray sources) may still take advantage of the enhancement via BRA.

As shown in Fig. 9a and d, at late times the BRA eventually decouples from the seed resulting in a loss of seed and wake amplitude. This decoupling can be attributed to the frequency and wavelength shifts in the seed pictured in Fig. 11.

FIG. 11. Longitudinal wavenumbers of electromagnetic fields vs time from 2D PIC Simulations (a) case “1”, (b) case “2”, showing a decoupling between pump and seed attributed to the red-shifting of the seed. Line **1** is the pump at k_0 , line **2** shows the mean wavenumber of the redshifting seed.

It has been shown³⁷ that a short laser pulse that propagates in plasma with a density profile due to the wake’s Langmuir wave, $\delta n_w/n_0$, will develop frequency shifts that can be described by :

$$\delta k_1 = -\frac{\omega_p^2 \tau}{2\omega_1 n_0} \frac{\partial \delta n_w}{\partial \zeta}, \quad \delta \omega_1 = \frac{\omega_p^2}{2\omega_1} \frac{\delta n_w}{n_0} + \delta k_1 v_{g1} \quad (7)$$

with $\delta k_1 = \partial_x \Phi = \partial_\zeta \Phi$ and $\delta \omega_1 = -\partial_t \Phi$, where $\Phi(\zeta, \tau) = -\omega_p^2 \delta n_w \tau / (2\omega_1 n_0)$. The characteristic linear dependence of the δk_1 in time, $\tau = t$ is clearly seen in SCPIC simulations and well reproduced by Eq.(7). The resulting red shift in the wavelength and frequency follows from the geometry of the wake Langmuir wave, i.e. the seed pulse propagates together with the front of the wake experiencing constant and predominantly positive density gradient [cf. Eq. (7)]. The theoretical curve in Fig. 12b has been calculated using Eqs. (1) and (7), by taking the average of the wave-vector shift (7) over the seed pulse length,

$$\langle \delta k_1 \rangle = l_s^{-1} \int_0^{l_s} d\zeta' \delta k_1(\zeta') = -k_0 \frac{\omega_p t}{6\pi^2} \frac{n_e}{n_c} |a_1(0)|^2, \quad (8)$$

where we assumed $k_p l_s = \pi$ and $v_{g1} \simeq c$.

FIG. 12. In the short pulse regime, case “1”: (a) Fields and density from 1D PIC and theory at $t = 4.9$ ps, theoretical curves overlaid in black. (b) Spectrum of transverse field from 1D PIC with theory from Eq. (8) shown in black. In the self-modulated regime, case “2”: (c) fields and density from 1D PIC at $t = 17.2$ ps and (d) spectrum of transverse field from 1D PIC. In both cases the initial seed amplitude is $a_1 = 0.205$, and initial seed duration is 30fs. Plasma density are respectively $n_e/n_c = 0.0035$ and $n_e/n_c = 0.015$. Both PIC simulations were run with a simulation domain of $600\mu\text{m}$, $60\text{cells}/\mu\text{m}$ resolution, and 128 particles/cell.

Note that the dramatic frequency cascading of the self-modulated pulse in Fig. 12d is entirely due to the coupling between the wake and subsequent stages of forward Raman scattering. This pulse never reaches intensities that would lead to relativistic self-focusing that is usually associated with the self-modulated regime³⁸.

To model the frequency shifts in the seed, the system of the 3-wave coupling equations¹⁰, Eqs. (2-4) has to be modified by introducing in Eq. (3) the frequency shift term $\delta\omega$. Equation (3) in the system Eqs. (2-4) is hence replaced by

$$[\partial_\tau + i\delta\omega] \hat{a}_1 = \gamma_0 a_0 a_L^* . \quad (9)$$

where $\delta\omega = \frac{\omega_p^2}{2\omega_1} \frac{\delta n_w}{n_0}$. This modification is necessary to account for the effects of the plasma wake on the BRA. For very short seed pulses as proposed in^{9,39} the wake can have dramatic effects leading to the loss of resonance between BRA modes.

Stationary solutions to Eqs. (2),(9), and (4) are closely reproduce PIC simulations and are displayed in Fig. 13b to illustrate the need for including wake generation into theories involving short laser pulses such as BRA.

We will demonstrate how BRA can be applied to enhance the plasma wake when a chirped pump is employed. In absence of a frequency mismatch, i. e. $\delta\omega = 0$ in Eq. (3), the waves satisfy the usual matching conditions, $\omega_0 = \omega_1 + \omega_L$, $\vec{k}_0 = \vec{k}_L + \vec{k}_1$ ($k_0 = -k_1 + k_L$ for backscatter, with $k_a = |\vec{k}_a|$, $a = 0, 1, L$). When we describe the application of BRA to wake enhancement, we will consider short pulses on the order of the plasma wavelength λ_p . Any application of the wave coupling model Eqs. (2-4) in description of BRA must include a nonlinearity of the wake where $\delta n_w \sim |a_1|^2$ in the phase shift of Eq. (7).

Figure 13a shows the results of SCPIC simulations at $t = 40$ ps for the seed pulse amplitude a_1 and the pump amplitude a_0 and for the normalized amplitude of the electrostatic field, a_L , associated with the wake and Langmuir waves participating in the BRA that are characterized by short wavelength and are concentrated in the front part of the seed pulse. For this simulation with $n_e/n_c = 0.0035$, the initial seed pulse duration is $\tau_L = 30$ fs measured as the FWHM of a Gaussian envelope, and the left-propagating laser pump amplitude $a_0 = 0.0091$ (case “1”). An important feature of our BRA application to enhance the plasma wake is the wavelength separation between two main Langmuir wave components, i.e. the wake and BRA excited perturbations. Our attempt to describe interactions, as seen in Figs. 13a and b, i.e. BRA and the wake generation, by means of the 3-wave coupling model, Eqs. (2), (3), and (4) can be well approximated by a function for the nonlinear shift in Eq. (3) of the following form,

$$\delta\omega = -g_1 \sqrt{n_e/n_c} \omega_p |\hat{a}_1|^2, \quad (10)$$

where the numerical constant $g_1 = 1/(12\pi)$ was calculated for a sin model of the seed envelope. Fig. 13b shows the results of this model compared with SCPIC results using numerical solutions to the 3-wave coupling model (line 3), and integrating Eq. 10 with the seed amplitude obtained from PIC (line 2). SCPIC simulations show decoupling between the pump a_0 and the seed \hat{a}_1 due to the nonlinear evolution of the seed. This more complicated and nonuniform (within the pulse) frequency shift is absent in the 3-wave coupling model which shows further growth of the seed before saturation, leading to a larger frequency shifting rate. Figure 14 shows the wake amplitude versus seed propagation time from 1D simulations for different conditions. Figure 14a line 2 illustrates the enhancement of the wake amplitude due to BRA coupling until the decoupling at $t = 40$ ps due to nonlinear evolution of the seed.

FIG. 13. For the case “1” with constant pump: (a) fields \hat{a}_1 and a_L from PIC at $t = 40$ ps; (b) spectrum of transverse electric field (containing both pump and seed components) from PIC and from theory; line 1: for constant pump (line at $k = k_0$), line 2: solution to Eq. (10) obtained from the amplitude of the seed in PIC, and line 3: solution to Eq. (10) obtained from a numerical solution to the 3-wave coupling model. For the ideally chirped pump: (c) fields \hat{a}_1 and a_L from PIC at $t = 75$ ps; (d) Spectrum of transverse electric field from PIC; line (1) : pump field spectrum prescribed by matching condition, solid line (2): seed spectrum obtained from Eq. (11). Both PIC simulations were run with a simulation domain of $600\mu\text{m}$, $60\text{cells}/\mu\text{m}$ resolution, and 128 particles/cell.

C. Chirping the Pump

To overcome this decoupling due to the shift in the seed, a frequency-chirped pump can be used. To first order, the frequency of the seed follows Eq. (7). In this approximation a linearly chirped pump³² can prolong coupling and increase wake production as shown in Fig. 14a line 3 illustrating the enhancement of the wake and delayed decoupling in this case. However, as the seed is amplified it produces a larger amplitude wake resulting in a non-linear change in frequency, and eventually a linearly chirped pump will not suffice to maintain coupling.

We can estimate this nonlinear frequency change by using Eq. (7). This expression can be easily modified to include the effects of Raman amplification through a linear amplitude growth rate^{9,12} by substituting $a_1(0)$ with $a_1(t) = a_1(0) (1 + bt)$, with b as a parameter. Substituting this into Eq. (8) and integrating leads to the following approximation of the seed’s wavenumber shift:

$$\langle \delta k_1 \rangle(t) = -\frac{k_p^3}{k_1(0)} \frac{v_{g1}}{6\pi} \left(a_1^2(0)t + a_1(0)b t^2 + \frac{1}{3}b^2 t^3 \right), \quad (11)$$

The pump frequency satisfies the usual matching conditions for coupling when $\omega_0(t) = \omega_0(0) + c \langle \delta k_1 \rangle(t)$, corresponding to a chirped pump with $\omega_0(0)$ as the unshifted frequency.

This result can also be obtained by applying similar steps to the theory given in Ref.⁴⁰. Equation (11) underestimates the rate of frequency reduction as it does not account for time evolution of the critical density defined by the changing seed pulse; however, by adjusting the parameter b , it was used to model the spectral evolution of the seed (Fig. 13d line 2) and to model a pump that would ensure coupling (Fig. 13d line 1). Figs. 13c and d and 14a line 4 demonstrate such a case where the seed and pump maintain coupling throughout the non-linear shifting process with the value of $b = 0.012\text{ps}^{-1}$. One can observe the strong wake enhancement in Fig. 14a line 4 as the seed's frequency approaches the plasma frequency, and the seed is slowed down dramatically. Fig. 13c shows a snapshot of the pulse and its wake at $t = 75\text{ps}$ giving a quantitative value for the electric fields, in this simulation $E_w \sim 4.5 \times 10^{10}\text{V/m}$. Strong electric fields such as these may be capable of reflecting, and accelerating ions⁴¹.

FIG. 14. Wake amplitude versus seed propagation time from 1D simulations for (a) short Gaussian pulses with parameters of case “1” and (b) self modulated pulses with parameters of case “2”. In (a), curves correspond to: **1** no pump, **2** constant pump, $\delta k_1 = 0$, **3** linearly chirped pump, δk_1 from Eq. (11) with $b = 0$ and **4** ideally chirped pump, δk_1 from Eq. (11) with $b = 0.012\text{ps}^{-1}$. In (b) curves correspond to: **1** no pump, **2** constant pump and **3** linearly chirped pump.

To compare our result with realistic experimental conditions, we will consider the instantiations phase of the pump required BRA for coupling. We note that in the presence of a shift in the seed and frequency chirped pump, the Langmuir frequency ω_L may deviate from resonance. However, since our parameters correspond to the superradiant regime^{9,35,36} ($\omega_{pe} \leq 2\omega_0\sqrt{a_0a_1}$) where there is increased bandwidth in the Langmuir waves, the interaction is still effective. To satisfy the wavenumber matching conditions $\vec{k}_0 = \vec{k}_L + \vec{k}_1$, one may use the average shift of the seed wavenumber (8) (cf Fig. 12b) to determine the instantaneous phase of the pump to sustain the original resonance condition: $\Phi_0(x, t) = \omega_0(t+x/c) + \alpha(t+x/c)^2/2$ with $\alpha = -\frac{\omega_0\omega_{pe}}{12\pi^2} \frac{n_e}{n_c} |a_1(0)^2|$, where α is the linear chirp coefficient, and has a value of $-2.3 \times 10^{23}\text{s}^{-2}$ for our standard parameters (“1”, “4”, “5”, “6”). Linear chirp coefficients up to $4.47 \times 10^{23}\text{s}^{-2}$ have been obtained in experiments³² and could be applied to maintain coupling.

When the effects of diffraction are completely overcome and the seed pulse amplitude grows in time, it is necessary to use the non-linear “ideal chirp” prescription (11) to maintain coupling. For early times ($t \leq 40\text{ps}$) the “ideal chirp” prescription is well approximated by the linear shift (cf. figure 14a line 3), but for long durations the non-linear shift is unlikely to be achieved by current CPA lasers. Density tapering⁴² could also potentially be used to extend the coupling duration between the pump and the seed. However, the increased plasma densities that are required also result in a greater red-shifting rate of the seed (Eq. 8), such that the seed's frequency evolution becomes non-linear and requires a very large, non-linear density gradient that is unlikely to be achieved in experiments.

IV. CONCLUSIONS

We have studied application of the BRA to the enhancement and control of the linear wake generation over a long plasma region. This has been achieved by energy transfer to a wake driving pulse via Raman coupling with a laser pump of low intensity and of long pulse duration. Using PIC simulations we have examined a wide range of background plasma conditions, as well as considered results of the previous BRA optimization studies²³. Wake generation favors low background electron density, such as $n_e = 0.0035n_c$, where it is possible for a 30fs laser seed pulse to have a FWHM comparable with half of a plasma wavelength $\lambda_p/2$. This optimal pulse length for wake generation at higher plasma densities would require shorter laser pulses and therefore will undermine the efficiency of the Raman amplification process. Also wakes at the lower densities are more effective for particle

acceleration¹ as e.g. they correspond to a longer dephasing length. The physics of particle acceleration using wakes that were studied in this paper will be considered next in a separate publication. We have examined a range of electron temperatures and focused on the experimentally relevant²⁸ choice of $T_e = 100$ eV. By varying electron temperature we could alter properties of the resonant Langmuir wave driven by the SRS. At $T_e = 100$ eV and $n_e = 0.0035n_c$ the k-vector of the plasma wave, $k_L \approx 0.46k_D$ and BRA operates in the kinetic regime of SRS²⁹⁻³¹. However, at the short seed pulse durations kinetic effects related to trapped particle dynamics are only relevant on much longer time scales than BRA coupling. In addition the strong linear Landau damping limits the growth of SRS of the pump wave thus allowing for the long scale plasma to be considered. With the above choice of plasma parameters we have proceeded to examine the role of BRA in countering the limitations imposed by diffraction of the seed pulse and extending the wake generation to plasmas that are longer than the dephasing length. For a range of experimentally relevant f-numbers, Fig. 10 summarizes results of 2D PIC simulations and demonstrates that BRA applied to wake generation can help maintain the wake amplitude of diffracting laser pulses.

A great deal of an initial theoretical insight and motivations for experimental measurements of BRA have been based on the solutions to the simple three wave coupling model⁹⁻¹¹. Such reduced models are useful in the understanding of BRA in large scale plasma experiments, provided diffraction of the laser pulses is not a factor and the effects of wake generation are included. We have demonstrated good agreement between PIC simulations and the reduced theoretical description at the early times of the BRA coupling. We have extended validity of the wave coupling models by accounting for the impact of the wake on the SRS coupling. This has been accomplished by including frequency and wavelength shifts in the electromagnetic seed equation that are caused by the time dependent, wake related, plasma inhomogeneities. The loss of the resonance coupling in the BRA that follows has been mitigated by introducing frequency chirp in the laser pump. Theory for the pump frequency chirp, in agreement with long time PIC simulations, showed the possibility of trapping the amplified laser seed pulse in a plasma. This results in a large increase in the wake amplitude and the generation of a shock like structure in the electrostatic field that will be further studied for the enhancement of particle acceleration.

ACKNOWLEDGMENTS

WR would like to thank Dr. P. Alves for useful discussions. JL and SW would like to thank Arthur Pak for useful discussions. JL is grateful for support from LLNL through the summer scholar program. JL and WR would like to acknowledge partial support from NSERC. SH is grateful to the CPHT computer support team.

¹E Esarey, C. B. Schroeder, and W. P. Leemans, *Rev. Modern Phys.* **81**, 1229 (2009).

²A. Rousse, K. Ta Phuoc, R. Shah, A. Pukhov, E. Lefebvre, V. Malka, S. Kiselev, F. Burgy, J-P. Rousseau, D. Umstadter, and D. Hulin, *Phys. Rev. Lett.* **93**, 135005 (2004)

³S. Kneip, C. McGuffey, J. L. Martins, S. F. Martins, C. Bellei, V. Chvykov, F. Dollar, R. Fonseca, C. Huntington, G. Kalintchenko, A. Maksimchuk, S. P. D. Mangles, T. Matsuoka, S. R. Nagel, C. A. J. Palmer, J. Schreiber, K. Ta Phuoc, A. G. R. Thomas, V. Yanovsky, L. O. Silva, K. Krushelnick and Z. Najmudin, *Nature Physics* **6**, 980 (2010).

⁴F. Albert and A. G. R. Thomas, *Plasma Phys. Control. Fusion* **58**, 103001 (2016).

⁵W. P. Leemans, C. G. R. Geddes, J. Faure, Cs. Tóth, J. van Tilborg, C. B. Schroeder, E. Esarey, G. Fubiani, D. Auerbach, B. Marcellis, M. A. Carnahan, R. A. Kaindl, J. Byrd, M. C. Martin, *Phys. Rev. Lett.*, **91**, 074802 (2003).

⁶Xi Zhang, V.N. Khudik, and G. Shvets, *Phys. Rev. Lett.* **114** 184801 (2015).

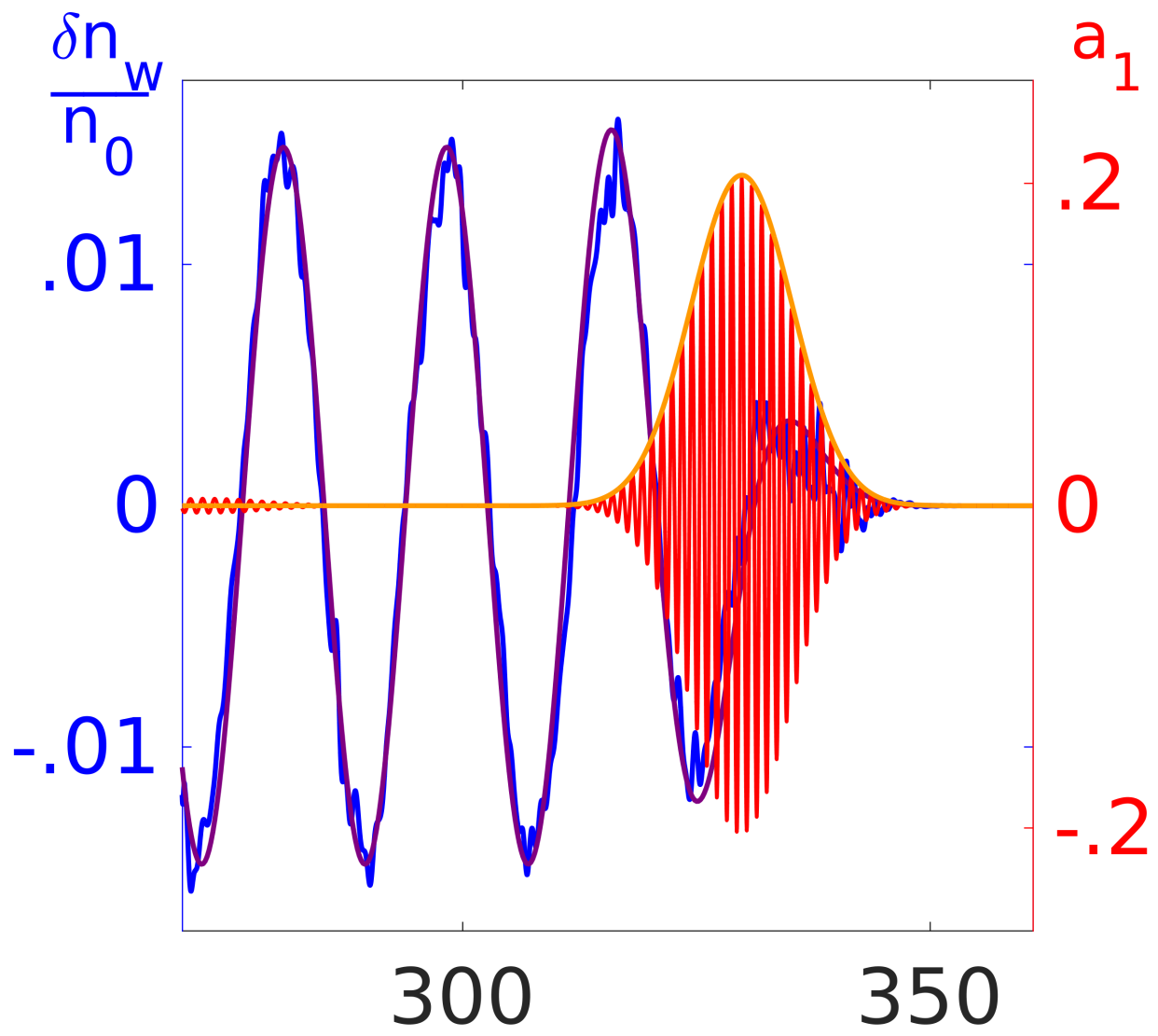
⁷S. Steinke, J. van Tilborg, C. Benedetti, C. G. R. Geddes, C. B. Schroeder, J. Daniels, K. K. Swanson, A. J. Gonsalves, K. Nakamura, N. H. Matlis, B. H. Shaw, E. Esarey and W. P. Leemans, *Nature* **530**, 190193 (2016).

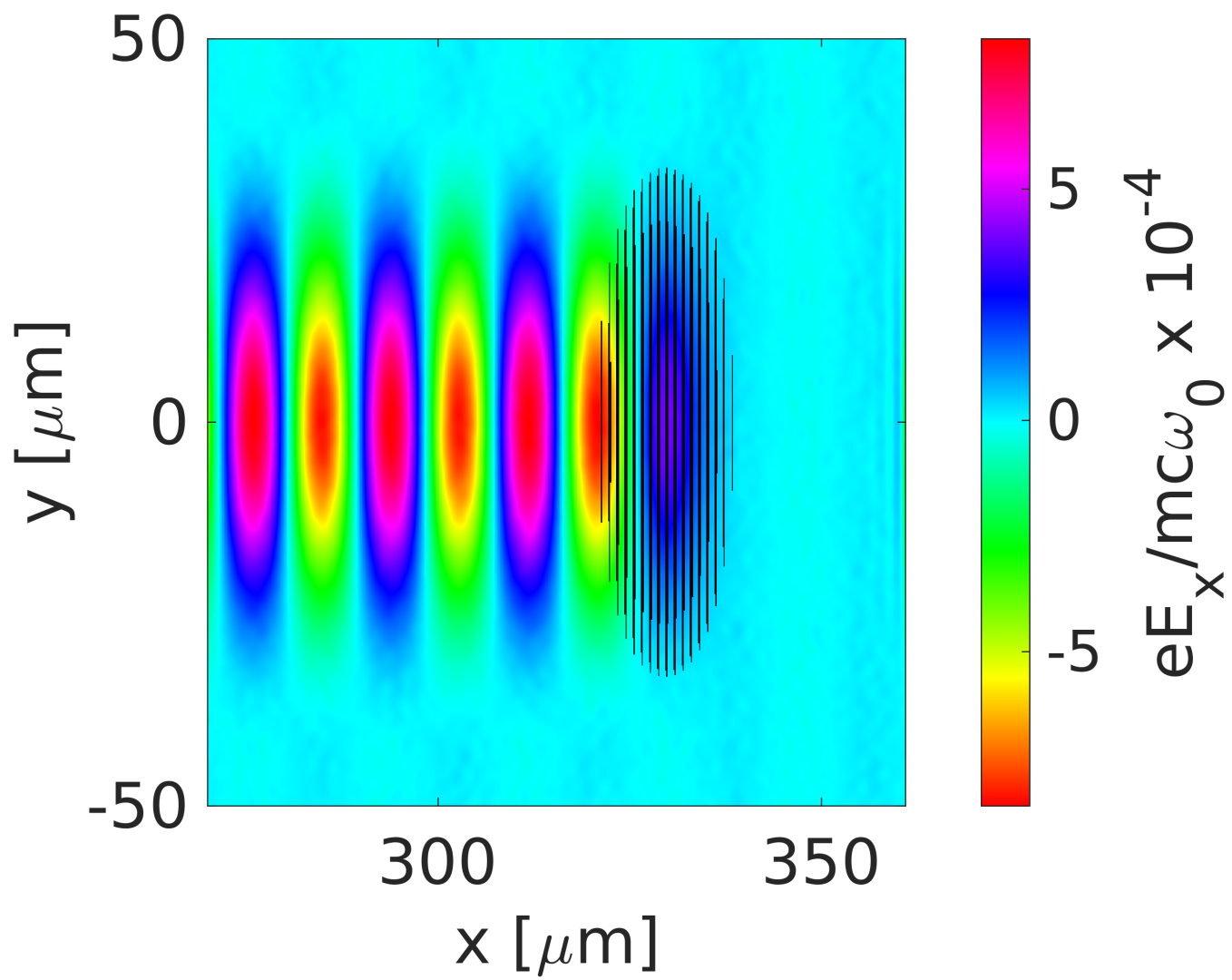
⁸J. Cowley, C. Thornton, C. Arran, R.J. Shalloo, L. Corner, G. Cheung, C.D. Gregory, S.P.D. Mangles, N.H. Matlis, D.R. Symes, R. Walczak, and S.M. Hooker, *Phys. Rev. Lett.* **119**, 044802 (2017).

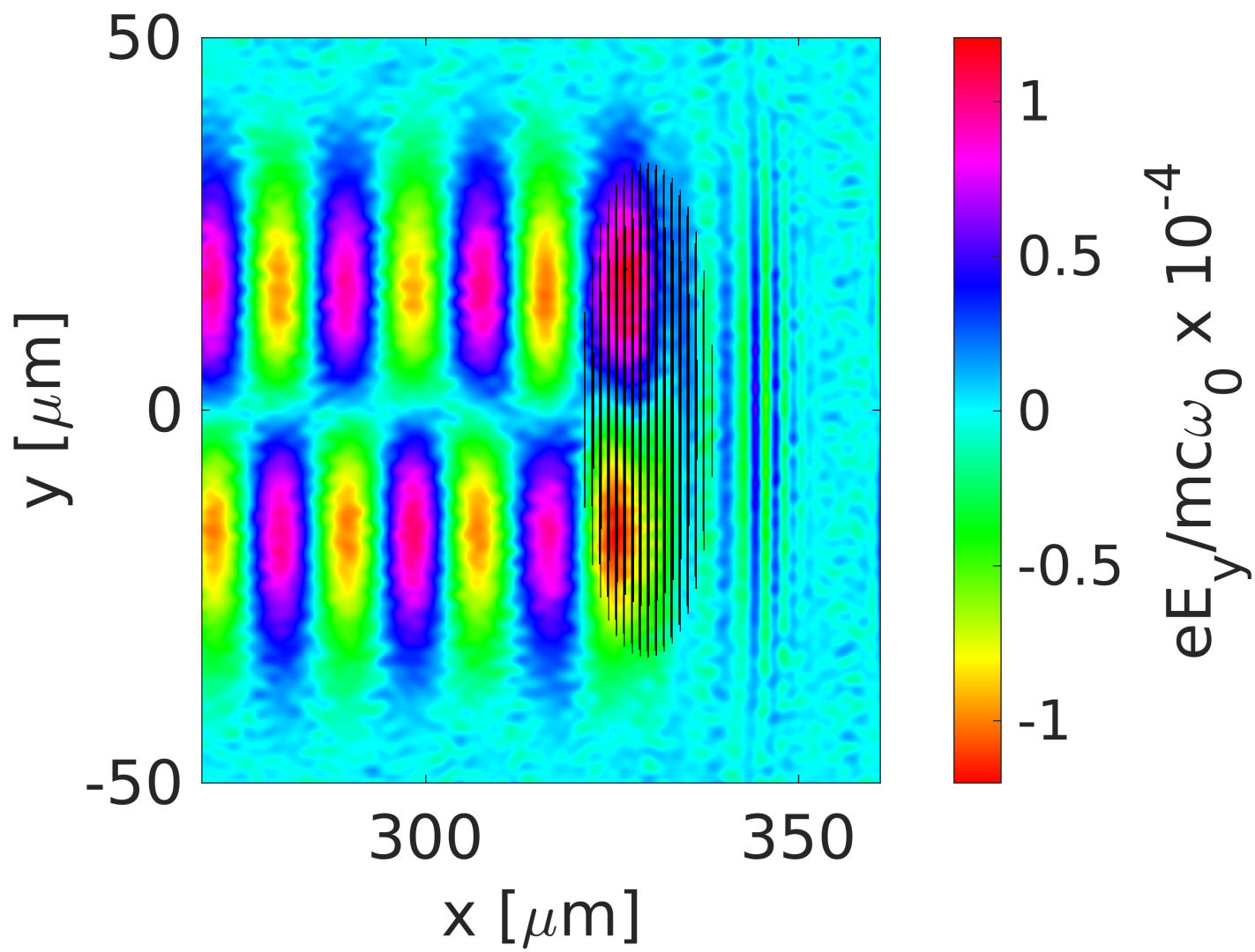
⁹G. Shvets, N. J. Fisch, A. Pukhov, and J. Meyer-ter-Vehn, *Phys. Rev. Lett.* **81**, 4879 (1998).

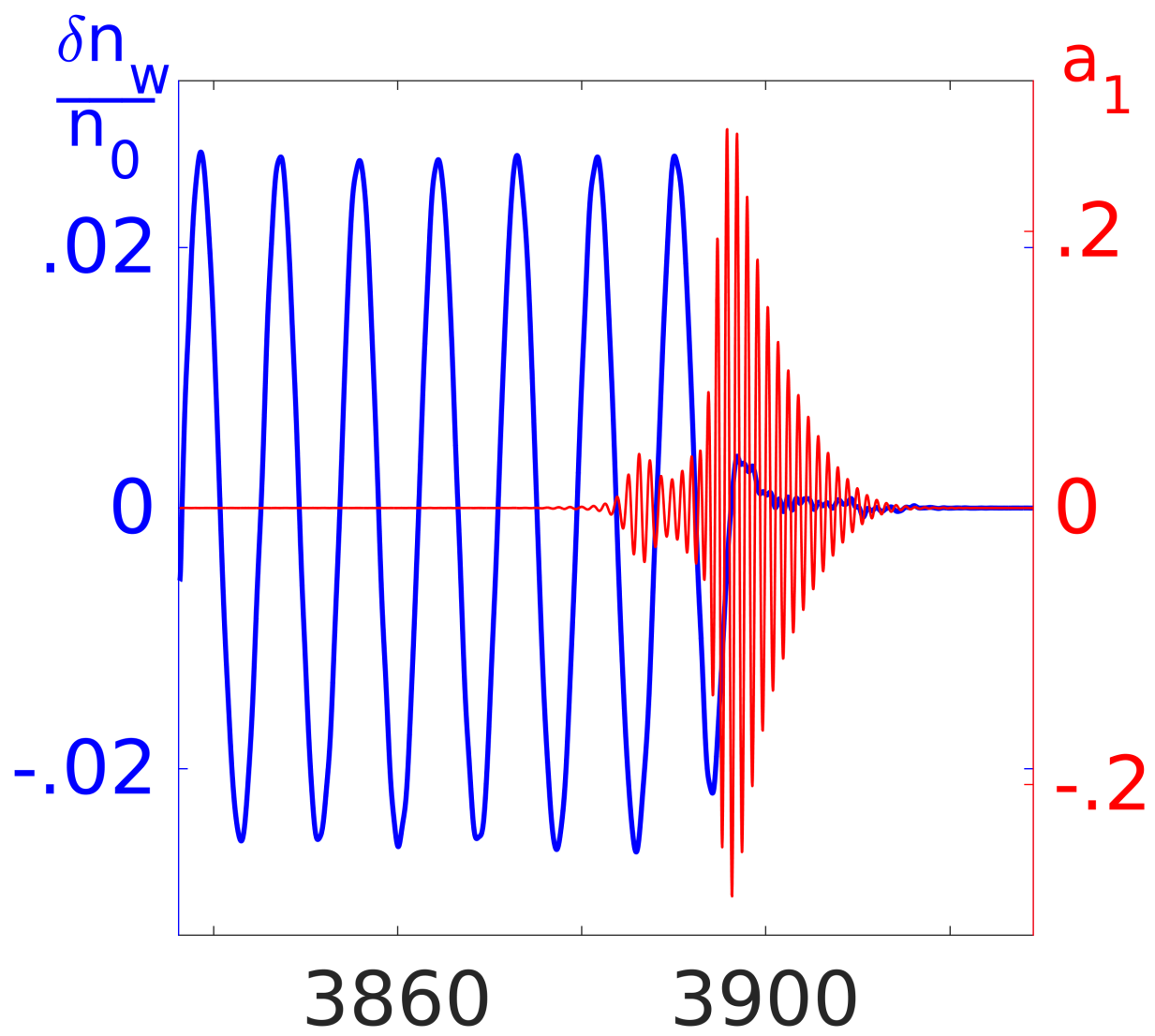
¹⁰V.M. Malkin, G. Shvets, and N.J. Fisch, *Phys. Rev. Lett.* **82**, 4448 (1999).

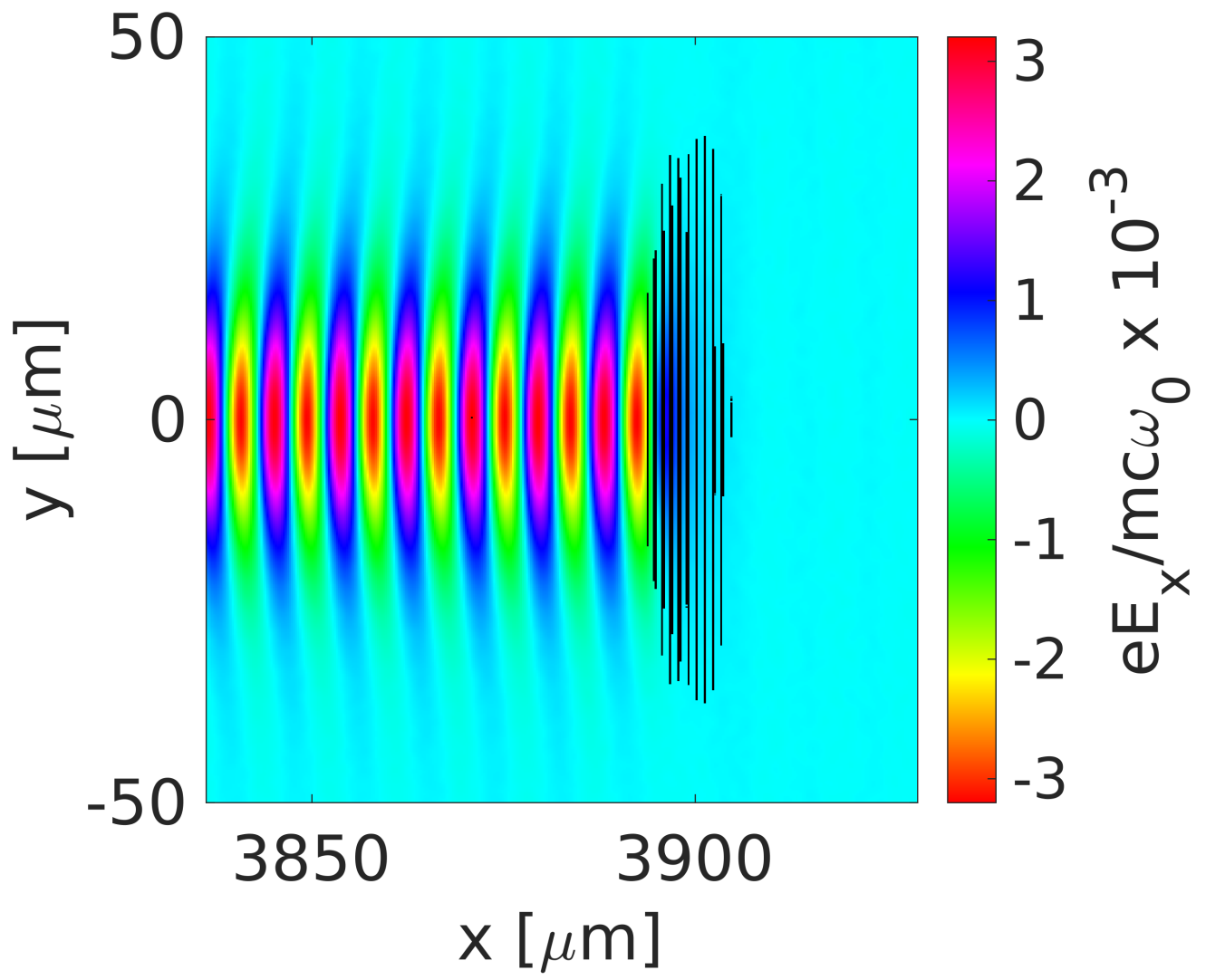
- ¹¹V.M. Malkin, G. Shvets, and N.J. Fisch, Phys. Rev. Lett. **84**, 1208 (2000).
- ¹²Y. Ping, W. Cheng, S. Suckewer, D.S. Clark, N.J. Fisch, Phys. Rev. Lett. **92**, 175007 (2004).
- ¹³Y. Ping, R. K. Kirkwood, T.-L. Wang, D. S. Clark, S. C. Wilks, N. Meezan, R. L. Berger, J. Wurtele, N. J. Fisch, V. M. Malkin, E. J. Valeo, S. F. Martins, and C. Joshi, Phys. Plasmas **16**, 123113 (2009).
- ¹⁴X. Yang, G. Vieux, E. Brunetti, B. Ersfeld, J. P. Farmer, M.S. Hur, R. C. Isaac, G. Raj, S.M. Wiggins, G.H. Welsh, S.R. Yoffe and D.A. Jaroszynski, Nature Scientific Reports **5**, 13333 (2015).
- ¹⁵D. Turnbull, S. Li, A. Morozov, and S. Suckewer, Phys. Plasmas **19**, 073103 (2012); *ibid* **19**, 083109 (2012).
- ¹⁶K. I. Popov, W. Rozmus, V. Yu. Bychenkov, N. Naseri, C.E. Capjack, and A. V. Brantov, Phys. Rev. Lett. **105**, 195002 (2010).
- ¹⁷D. V. Romanov, V. Y. Bychenkov, W. Rozmus, C. E. Capjack, and R. Fedosejevs, Phys. Rev. Lett. **93**, 215004 (2004).
- ¹⁸A. G. Mordovanakis, P.-E. Masson-Laborde, J. Easter, K. I. Popov, B. Hou, G. Mourou, W. Rozmus, M. G. Haines, J. Nees, K. Krushelnick, Appl. Phys. Lett. **96**, 071109 (2010).
- ¹⁹N. Naseri, D. Pesme, W. Rozmus, and K. Popov, Phys. Rev. Lett. **118**, 055002 (2012).
- ²⁰P. E. Masson-Laborde, M. Z. Mo, A. Ali, S. Fourmaux, P. Lassonde, J. C. Kieffer, W. Rozmus, D. Teychenné, R. Fedosejevs, Phys. Plasmas **21**, 123113 (2014).
- ²¹N. Naseri, D. Pesme, W. Rozmus, Phys. Plasmas **20**, 103121 (2013).
- ²²T.-L. Wang, D. Michta, R. R. Lindberg, A. E. Charman, S. F. Martins, and J. S. Wurtele, Phys. Plasmas **16**, 123110 (2009).
- ²³T. L. Wang, D. S. Clark, D. J. Strozzi, S. C. Wilks, S. F. Martins, and R. K. Kirkwood, Phys. Plasmas **17**, 023109 (2010).
- ²⁴R. Nuter, V.T. Tikhonchuk, Phys. Rev. E **87**, 043109 (2013).
- ²⁵P. Sprangle, E. Esarey, A. Ting, and G. Joyce, Appl. Phys. Lett. **53**, 2146 (1988).
- ²⁶D. Turnbull, S. Bucht, A. Davies, D. Haberberger, T. Kessler, J. L. Shaw, and D. H. Froula, Phys. Rev. Lett. **120** 024801 (2018).
- ²⁷R.M.G.M. Trines, E.P. Alves, E. Webb, J. Vieira, F. Fiuza, R.A. Fonseca, L.O. Silva, J. Sadler, N Ratan, L. Ceurvorst, M.F. Kasim, M. Tabak, D. Froula, D. Haberberger, P.A. Norreys, R.A. Cairns, R. Bingham, Phys. Rev. E **95**, 053211 (2017).
- ²⁸D. Haberberger, J. Katz, S. Bucht, A. Davies, J. Bromage, J.D. Zuegel, D.H. Froula, R. Trines, R. Bingham, J. Sadler, P.A. Norreys, Bulletin APS **62** (12), DPP:TO8.7 (2017).
- ²⁹H. A. Rose and L. Yin, Phys. Plasmas **15**, 042311 (2008).
- ³⁰P. E. Masson-Laborde, W. Rozmus, Z. Peng, D. Pesme, S. Hüller, M. Casanova, V. Yu. Bychenkov, T. Chapman, and P. Loiseau, Phys. Plasmas **17**, 092704 (2010).
- ³¹R. L. Berger, S. Brunner, J. W. Banks, B. I. Cohen, and B. J. Winjum, Phys. Plasmas **22**, 055703 (2015).
- ³²G. Vieux, A. Lyachev, X. Yang, B. Ersfeld, J. P. Farmer, E. Brunetti, R. C. Issac, G. Raj, G. H. Welsh, S. M. Wiggins and D. A. Jaroszynski, New. J. Phys. **13**, 063042 (2011).
- ³³C. Riconda, S. Weber, L. Lancia, J.-R. Marquès, G. A. Mourou, and J. Fuchs, Phys. Plasmas **20**, 083115 (2013).
- ³⁴A. Andreev, C. Riconda, V. Tikhonchuk, and S. Weber, Phys. Plasmas **13**, 053110 (2006).
- ³⁵B. Ersfeld and D. A. Jaroszynski Phys. Rev. Lett. **95** 165002 (2005).
- ³⁶D. A. Jaroszynski, P. Chaix, N. Piovella, D. Oepts, G. M. H. Knippels, A. F. G. van der Meer, and H. H. Weits, Phys. Rev. Lett. **78**, 1699 (1997).
- ³⁷E. Esarey, A. Ting, and P. Sprangle, Phys. Rev. A **42**, 3526 (1990).
- ³⁸C. I. Moore, A. Ting, K. Krushelnick, E. Esarey, R. F. Hubbard, B. Hafizi, H. R. Burris, C. Manka, and P. Sprangle, Phys. Rev. Lett. **79**, 3909 (1997).
- ³⁹V.M. Malkin, and N.J. Fisch, Eur. Phys. J. Special Topics **223**, 1157 (2014).
- ⁴⁰B. A. Shadwick, C. B. Schroeder, and E. Esarey, Phys. Plasmas **16**, 056704 (2009).
- ⁴¹F. Fiuza, A. Stockem, E. Boella, R. A. Fonseca, and L. O. Silva, Phys. Rev. Lett. **109**, 215001 (2012).
- ⁴²M. Chiamarello, F. Amiranoff, C. Riconda, and S. Weber Phys. Rev. Lett. **117**, 235003 (2016).

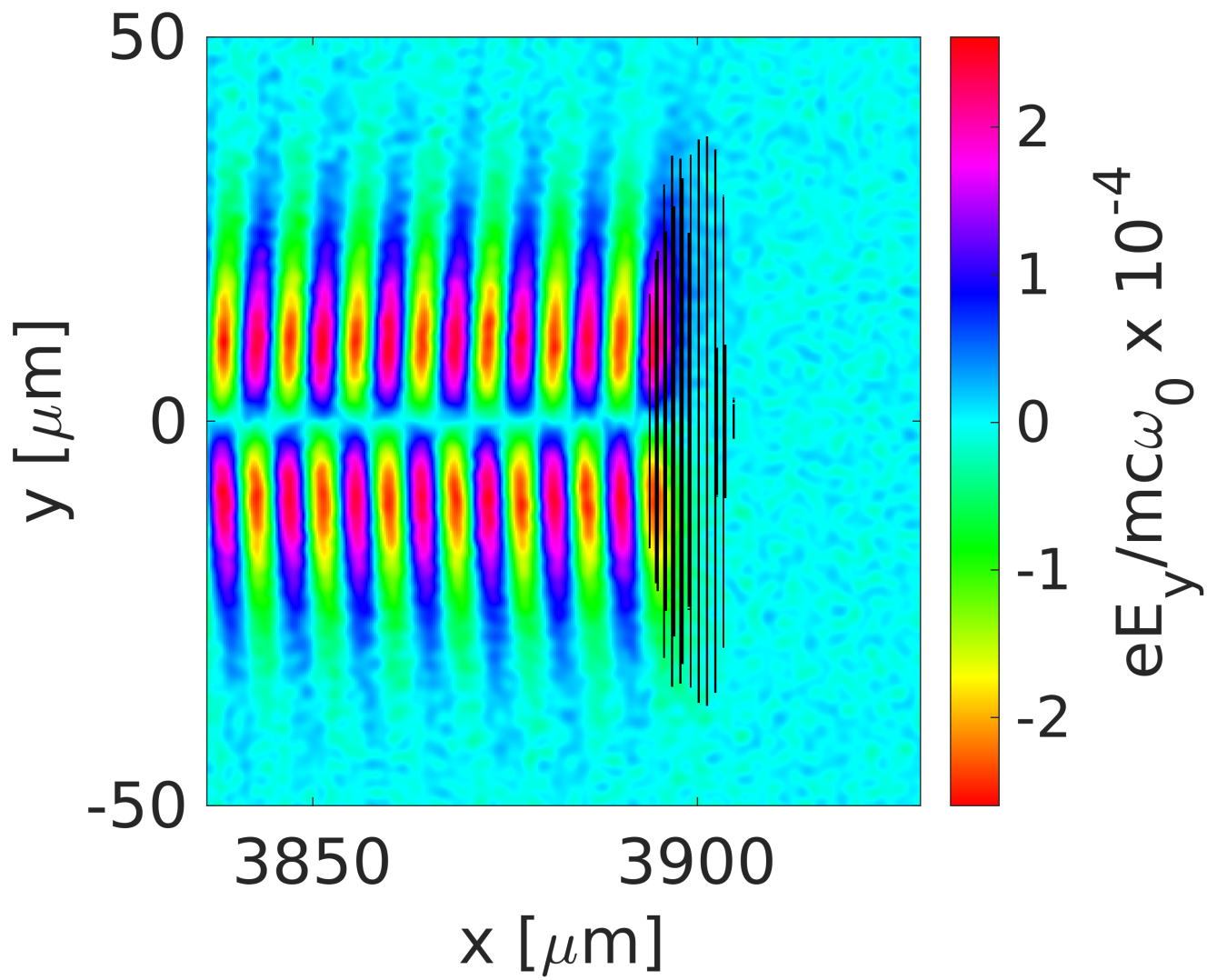


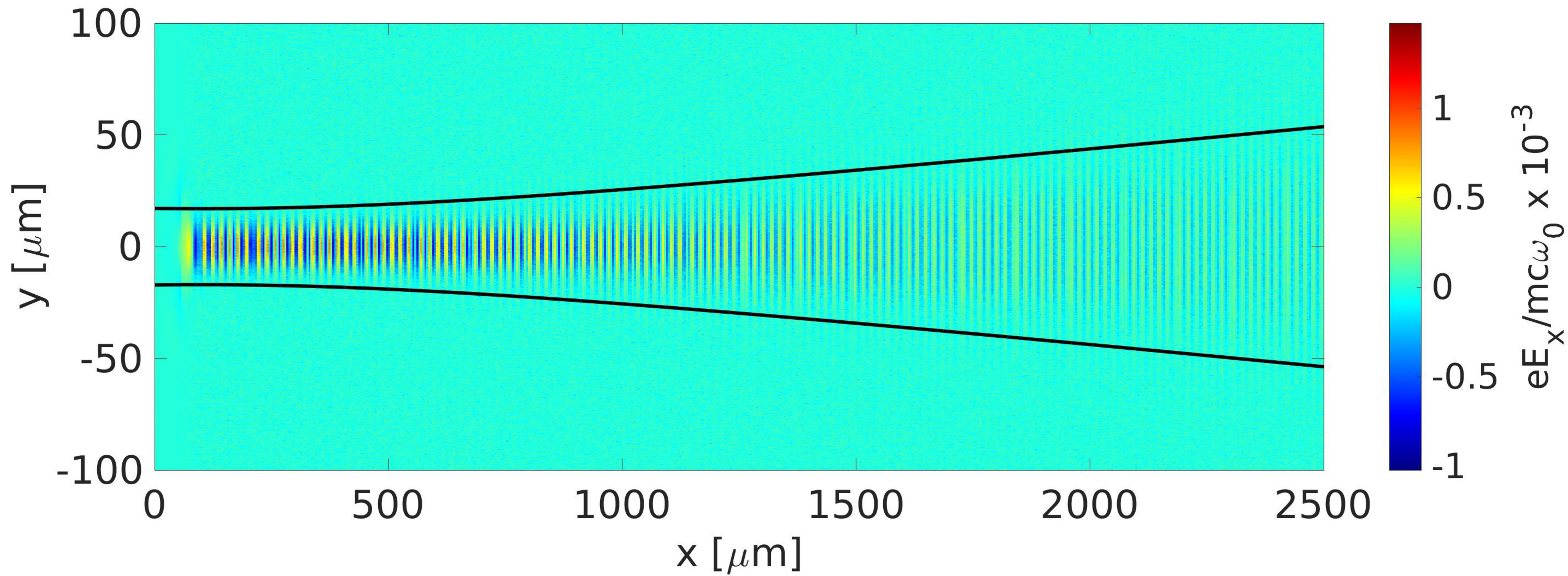


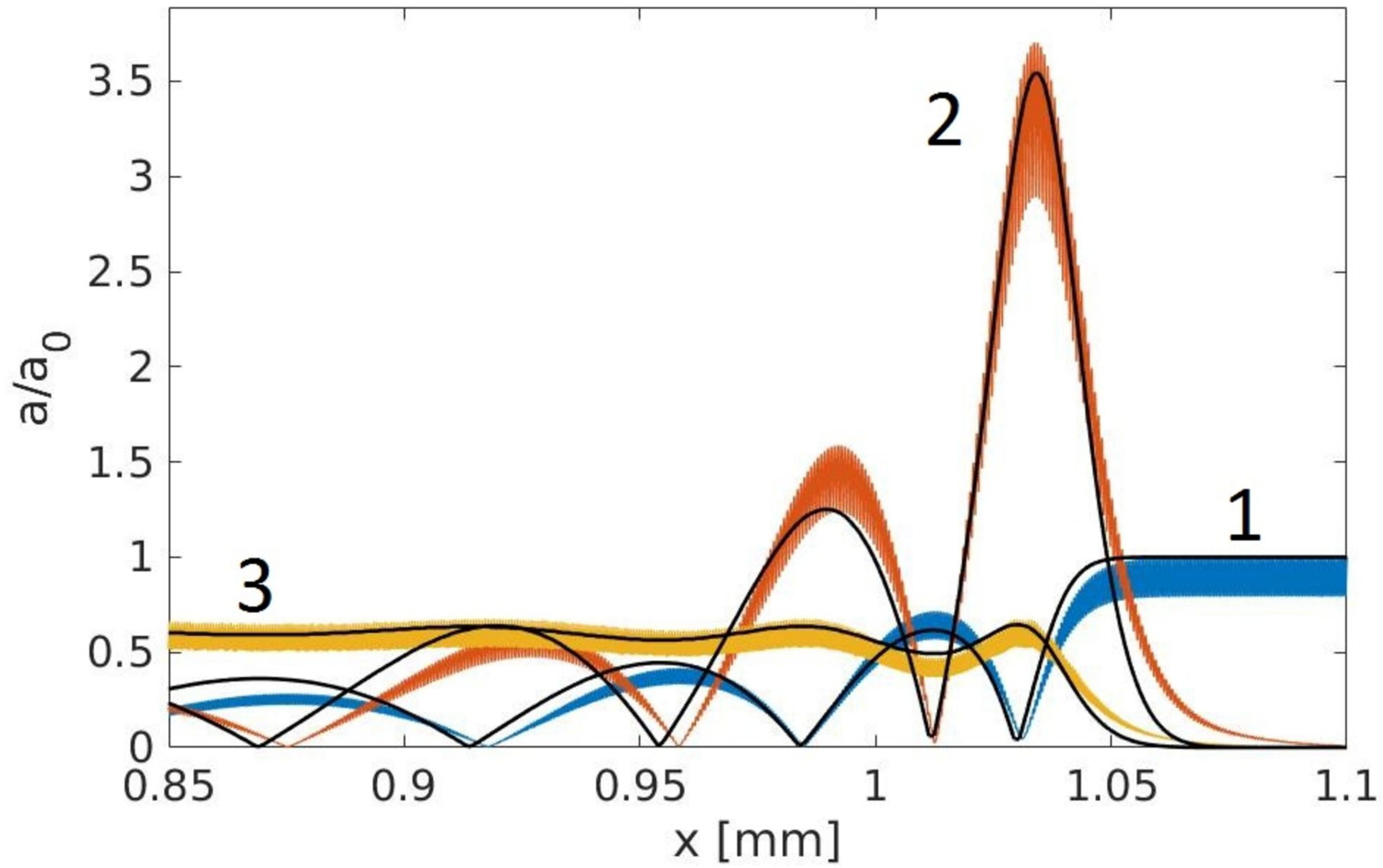


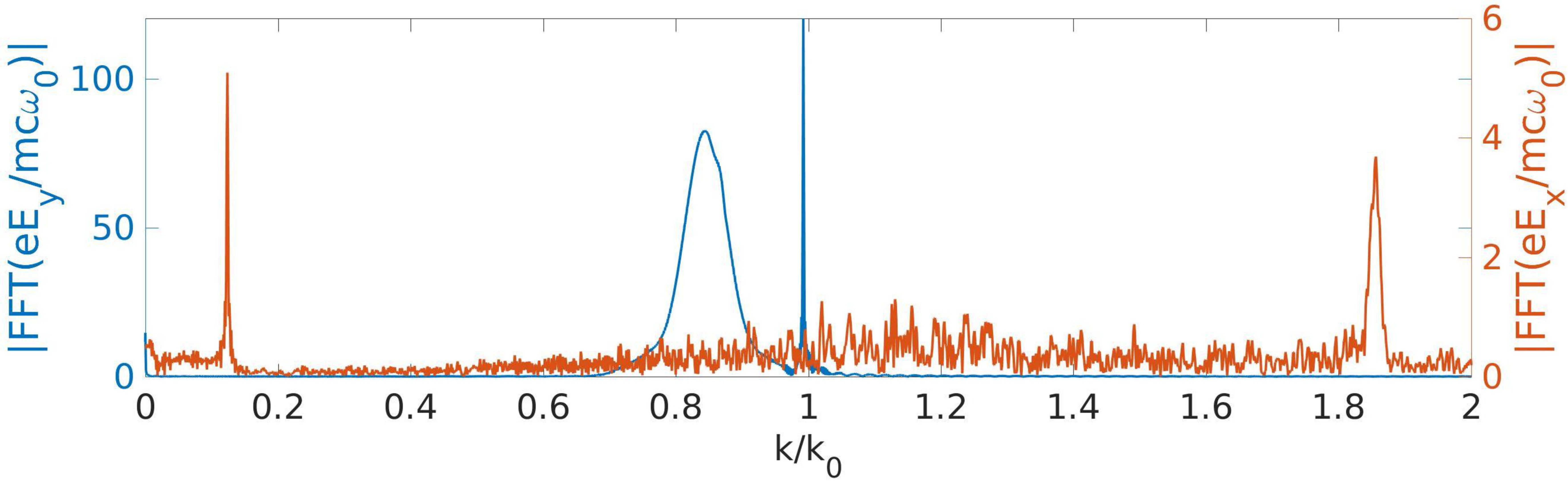


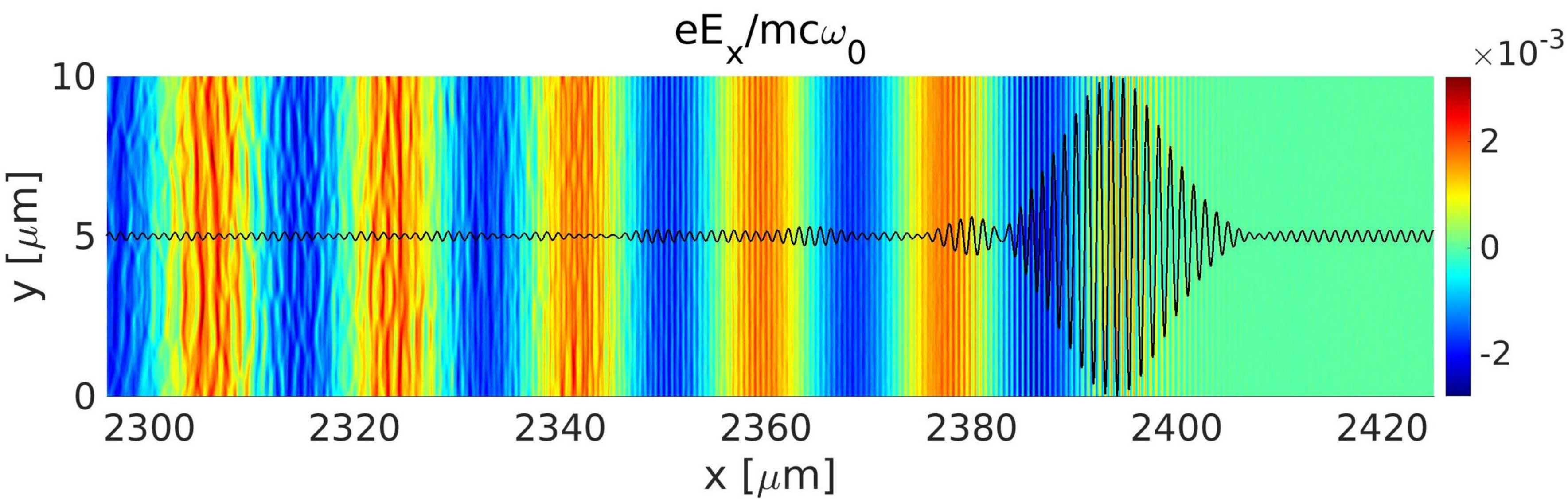


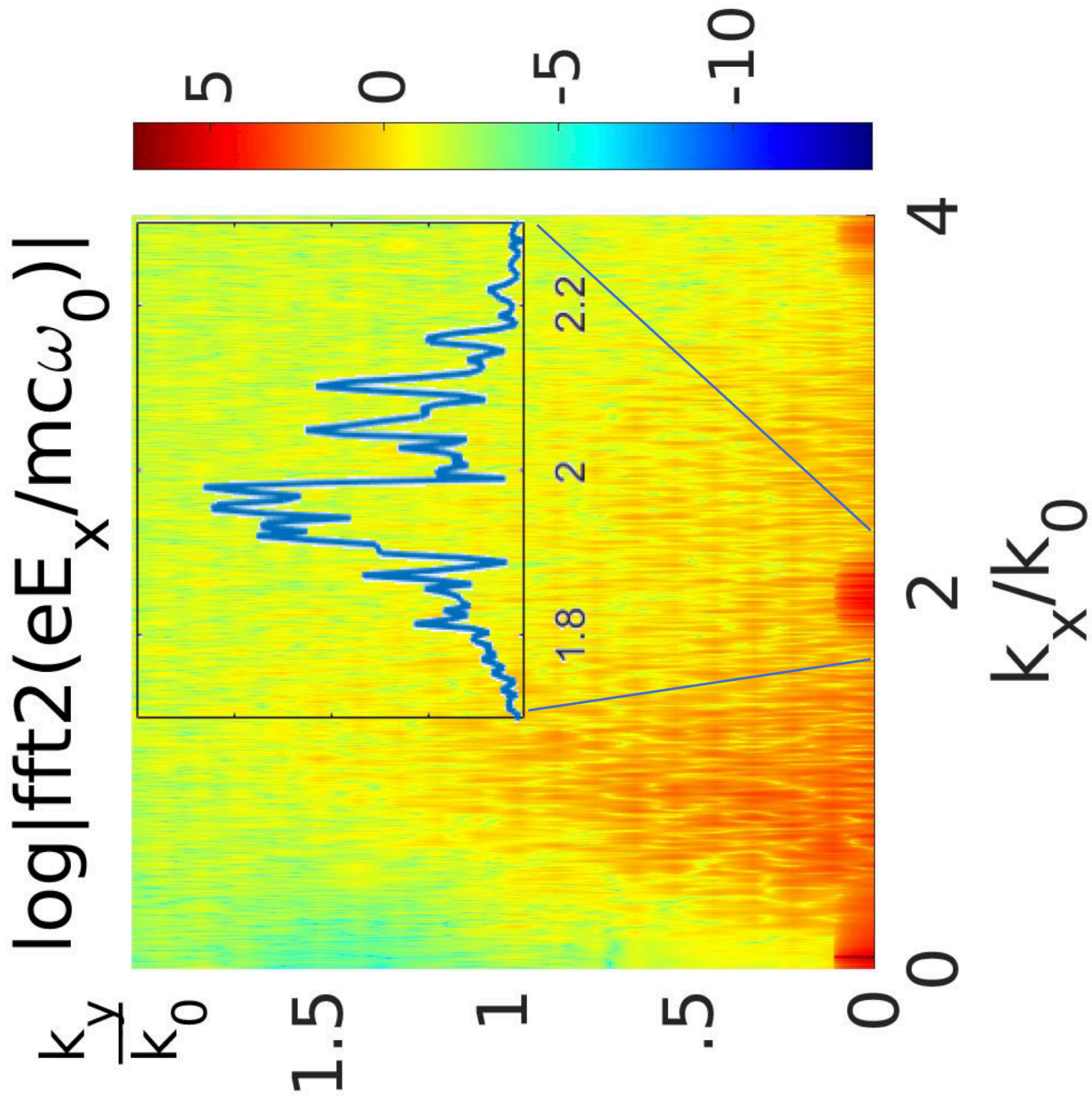




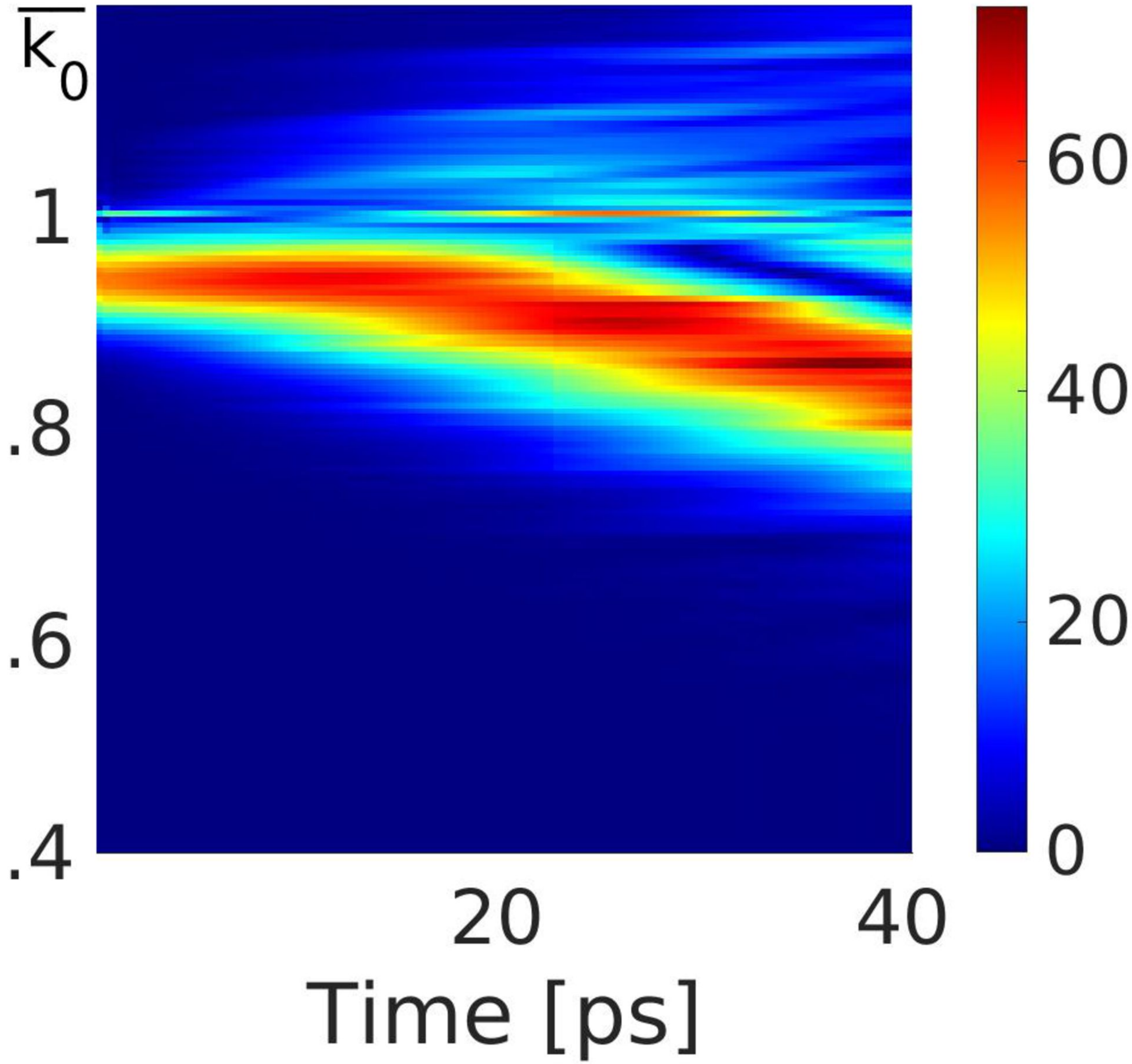


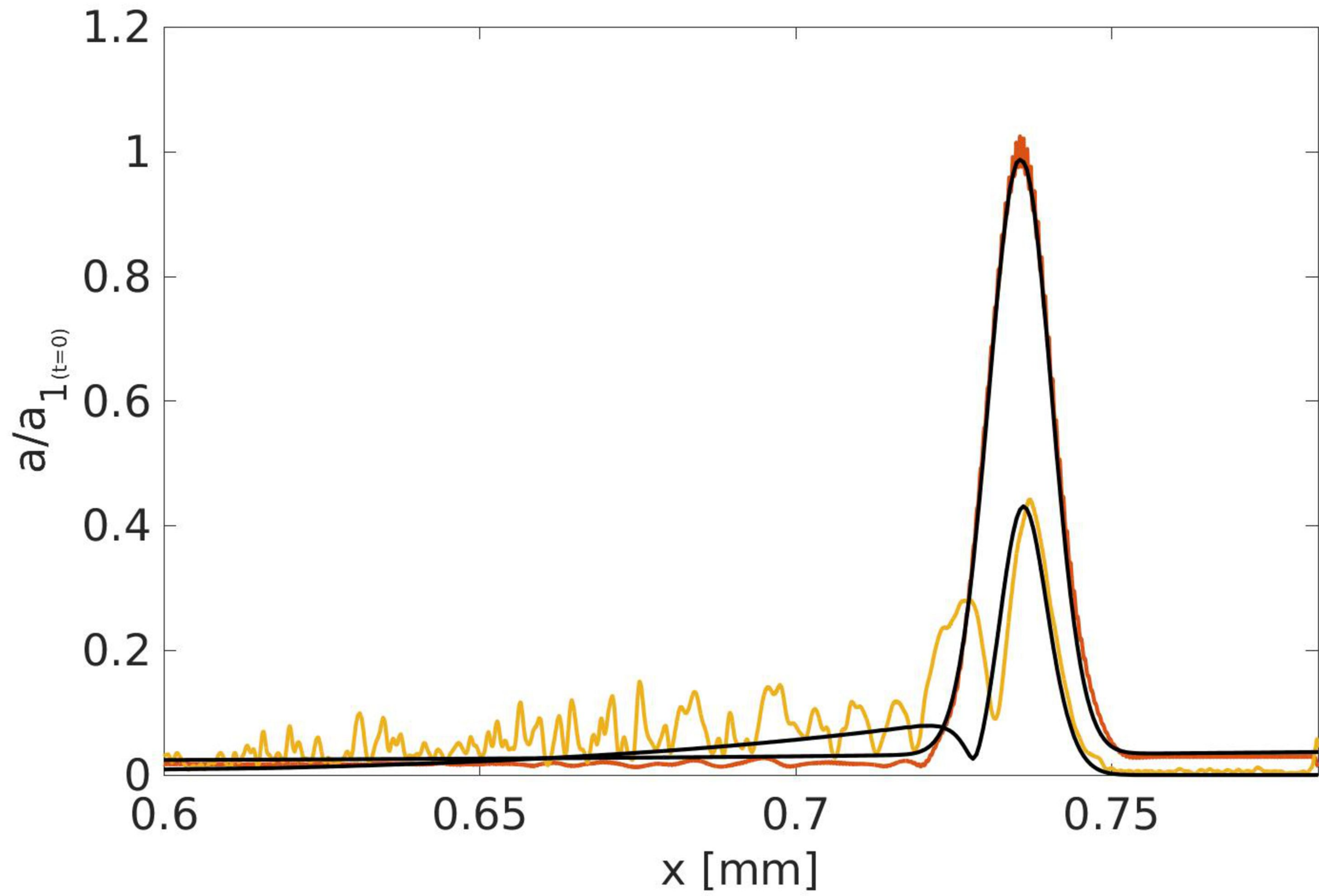


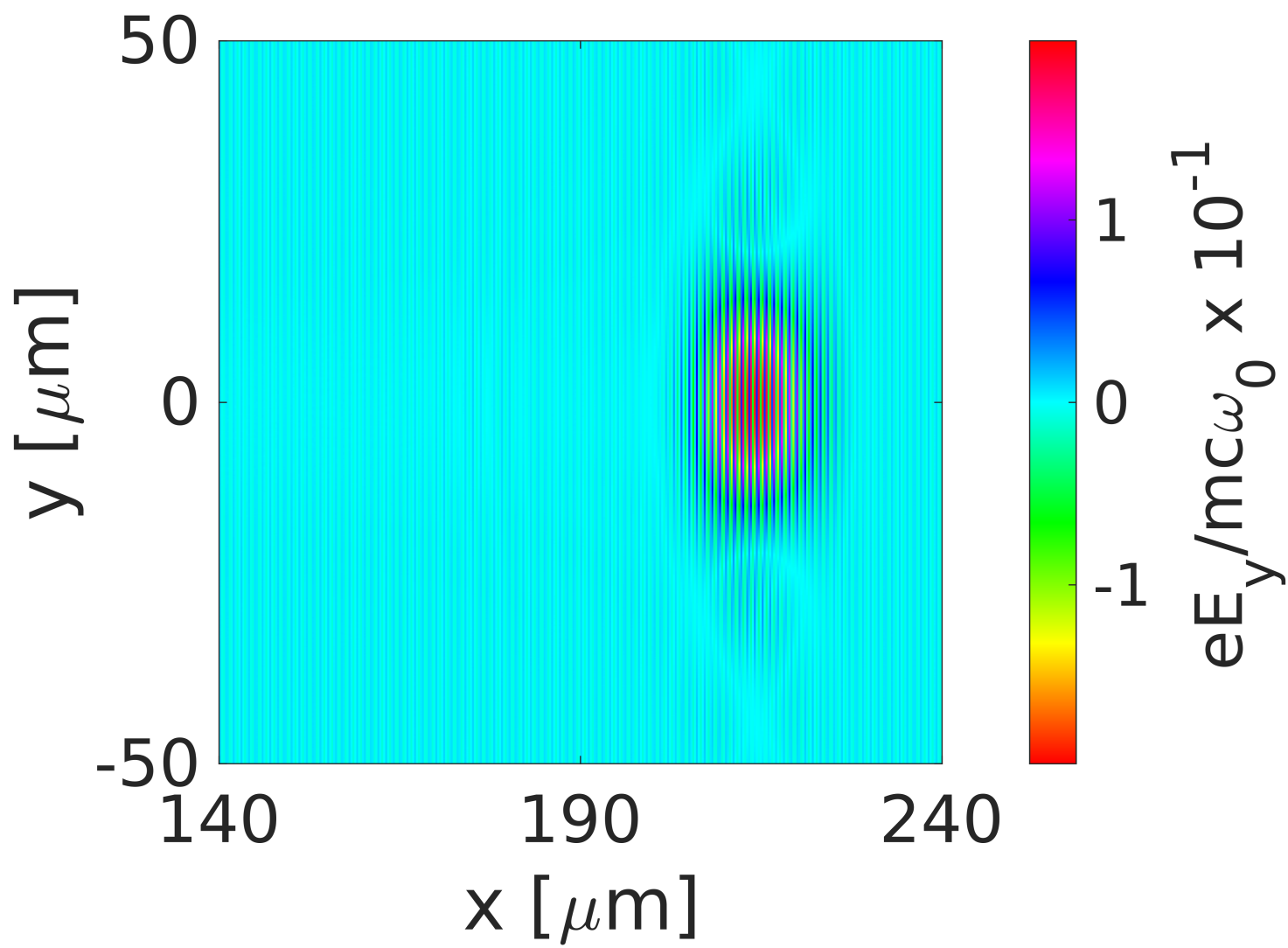


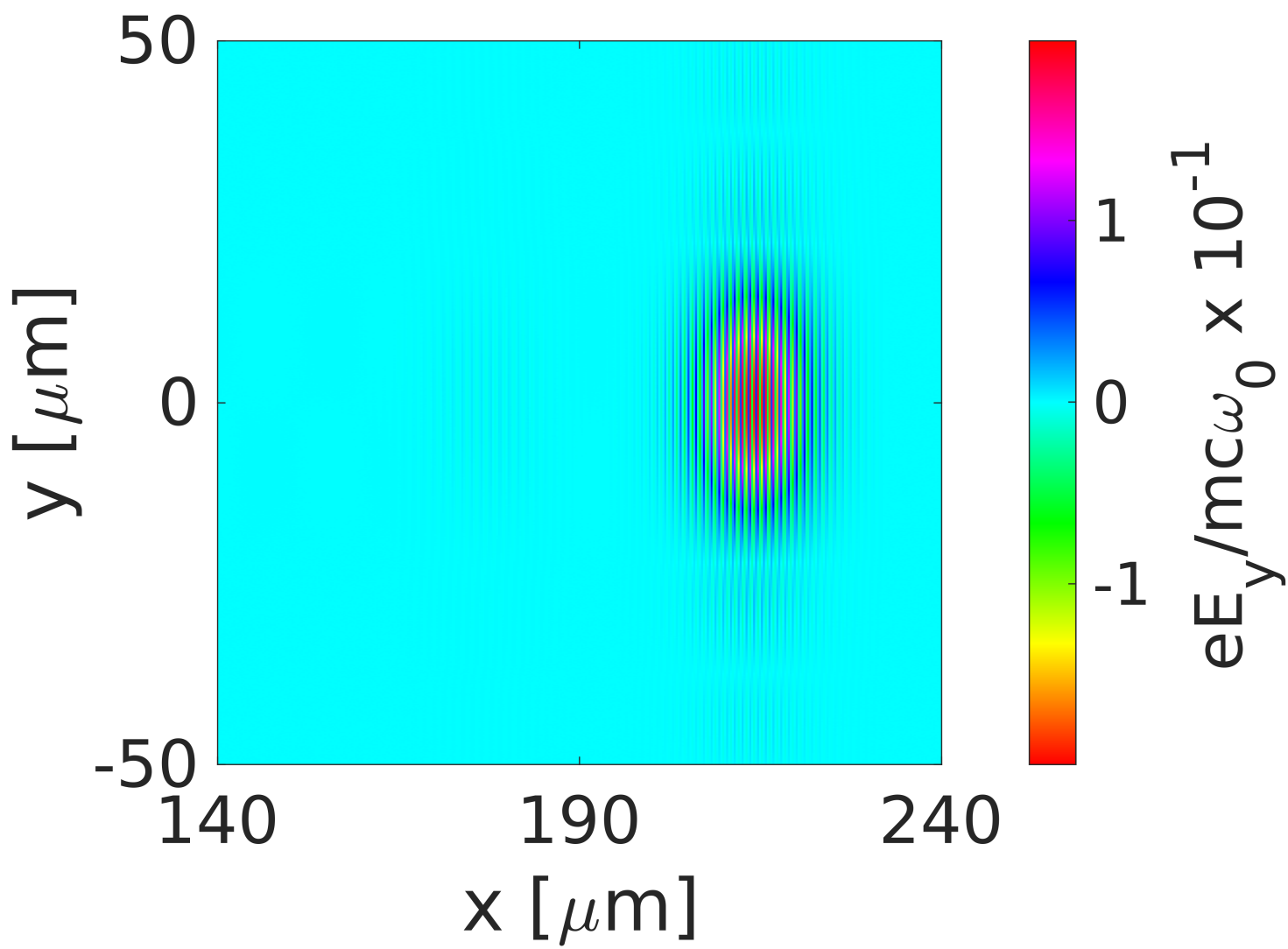


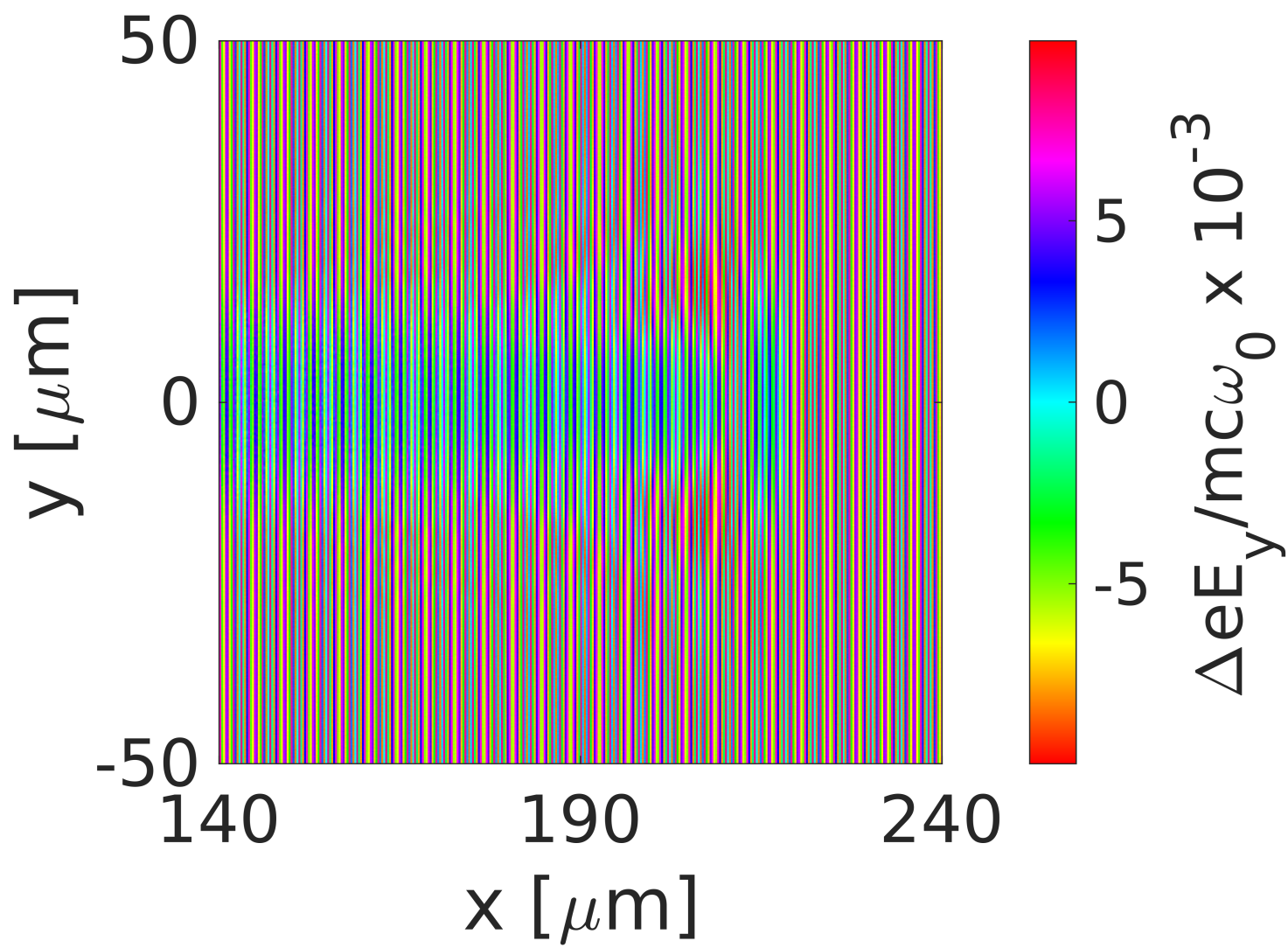
$$|\text{fft}(eE_y/mc\omega_0)|$$

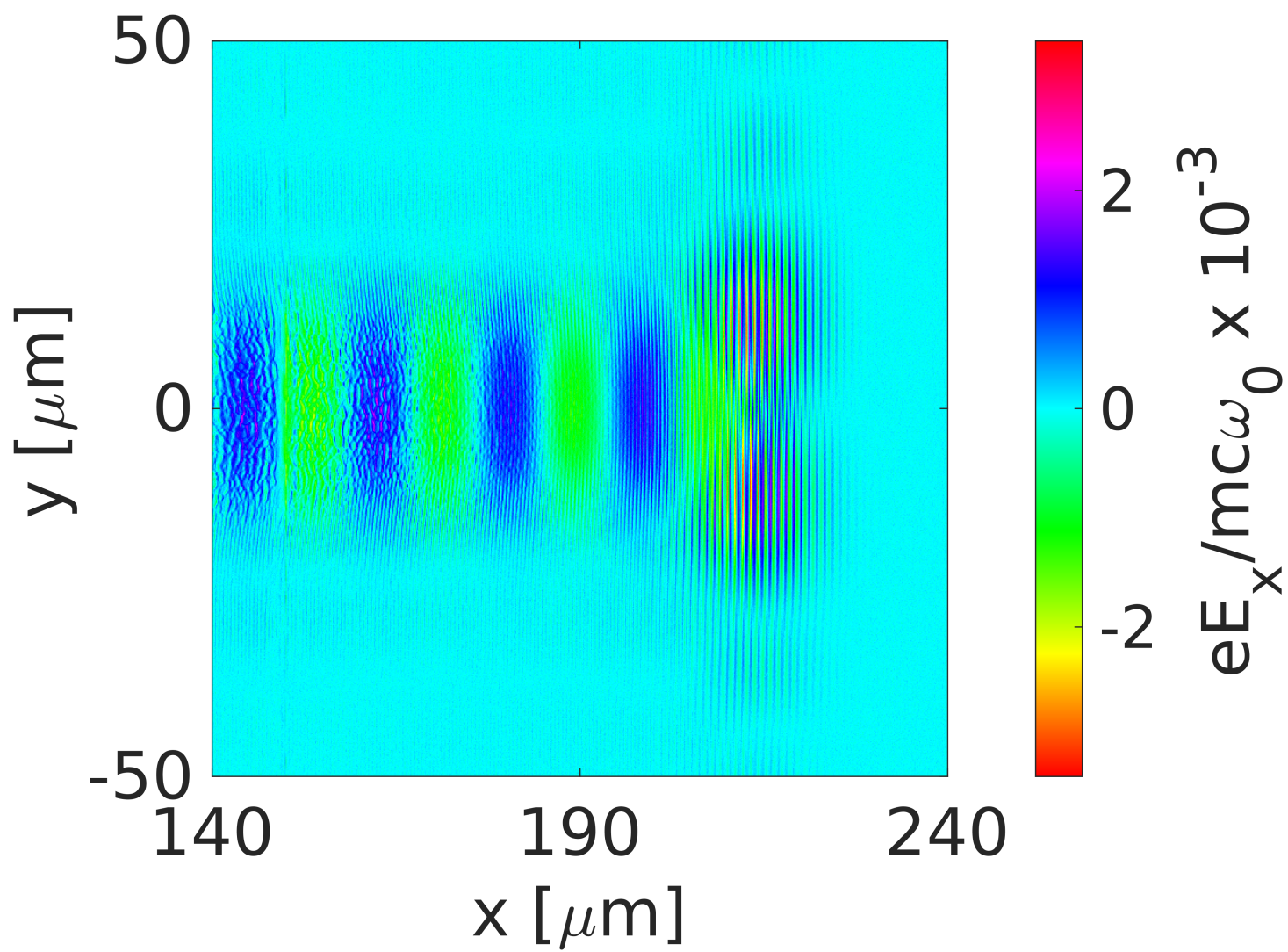


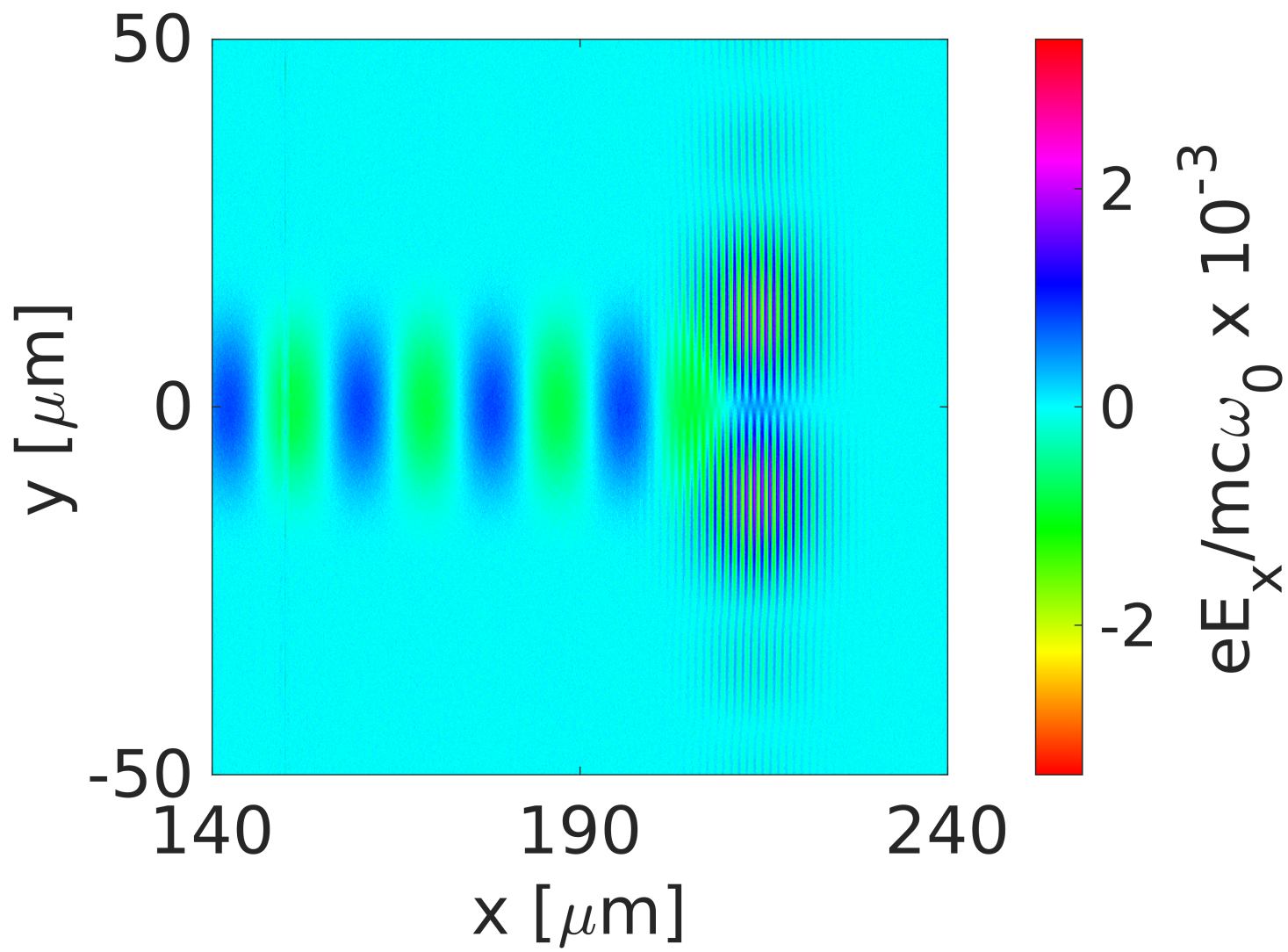


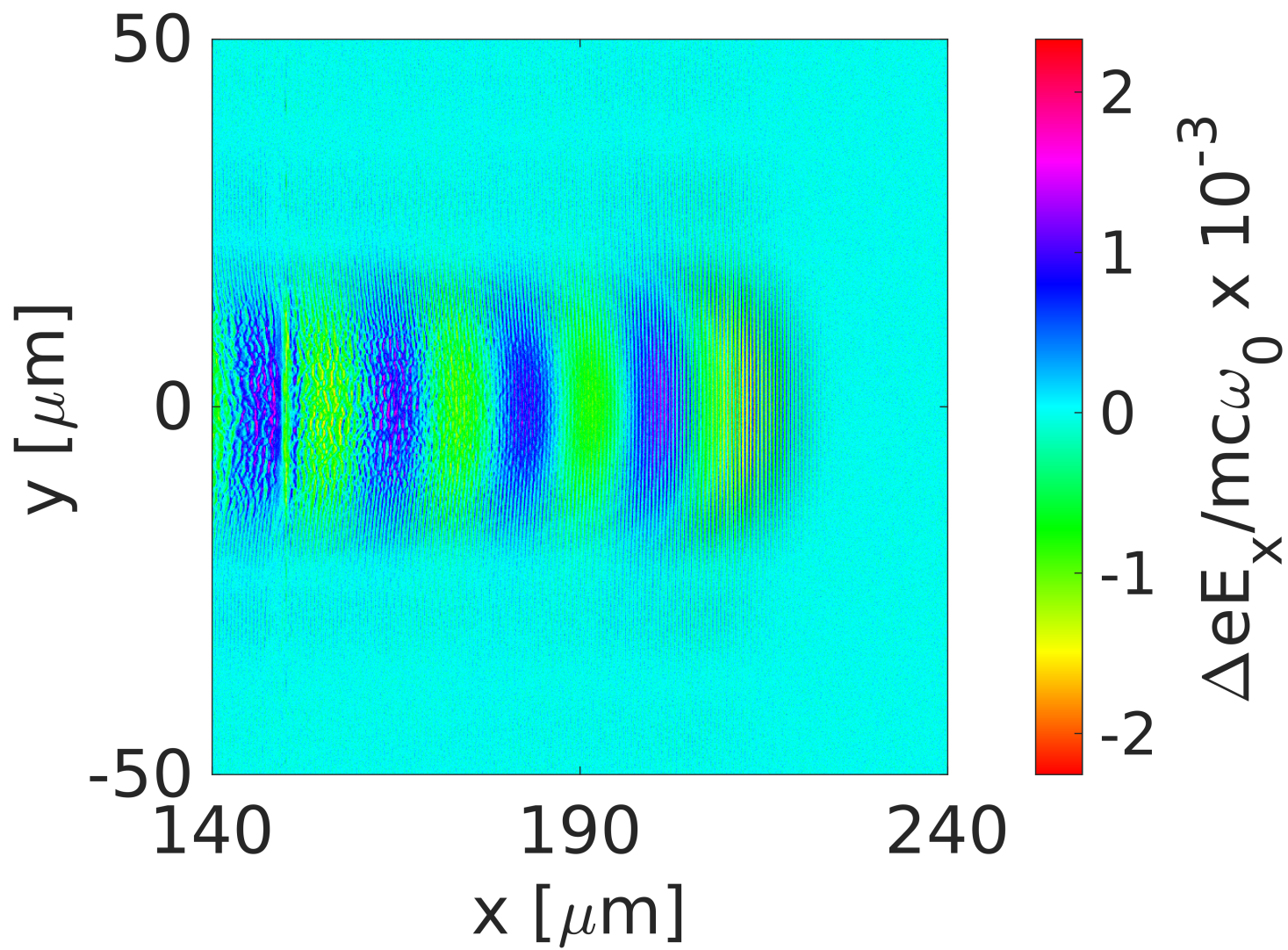


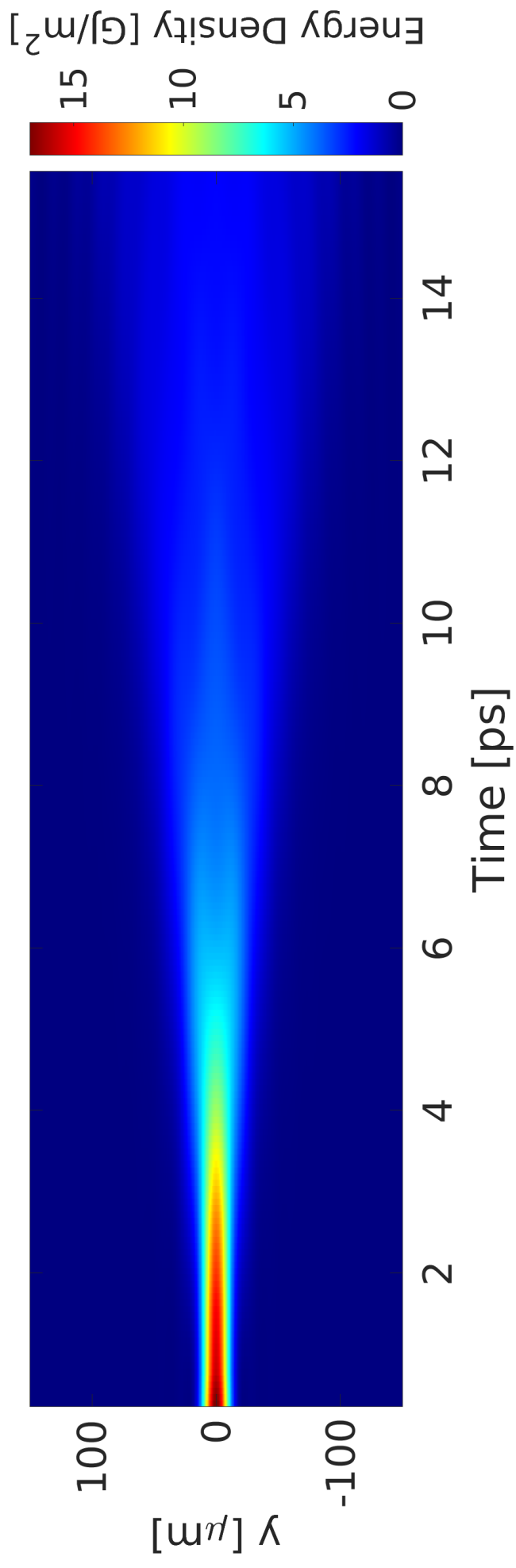


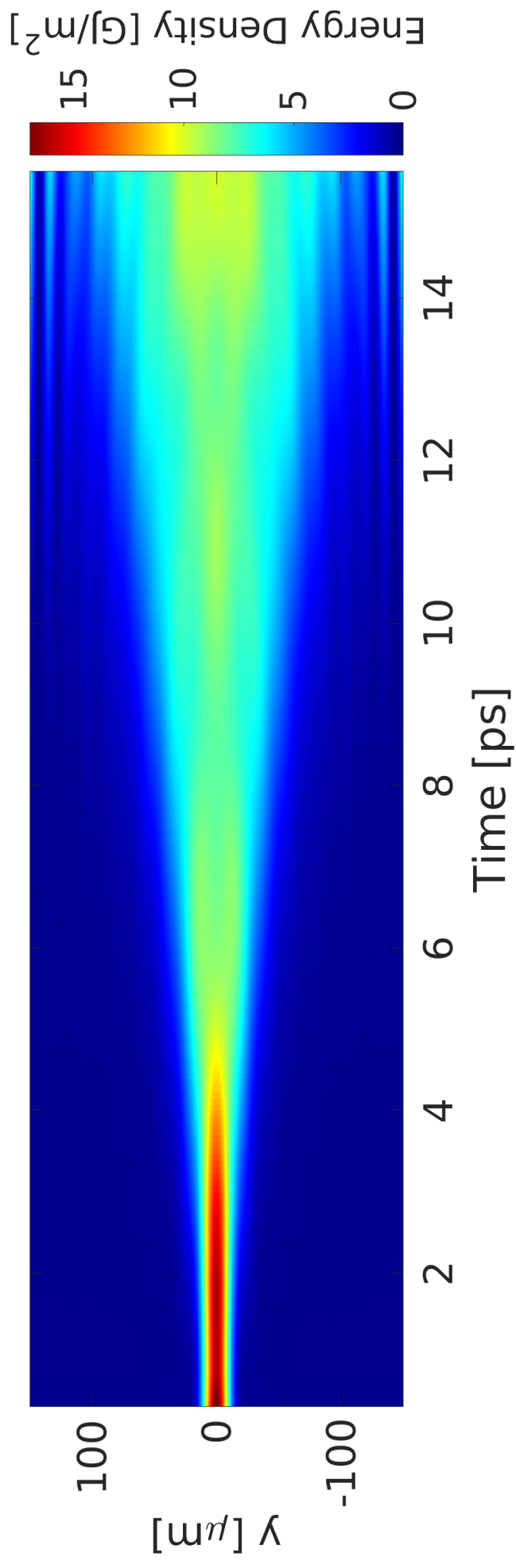




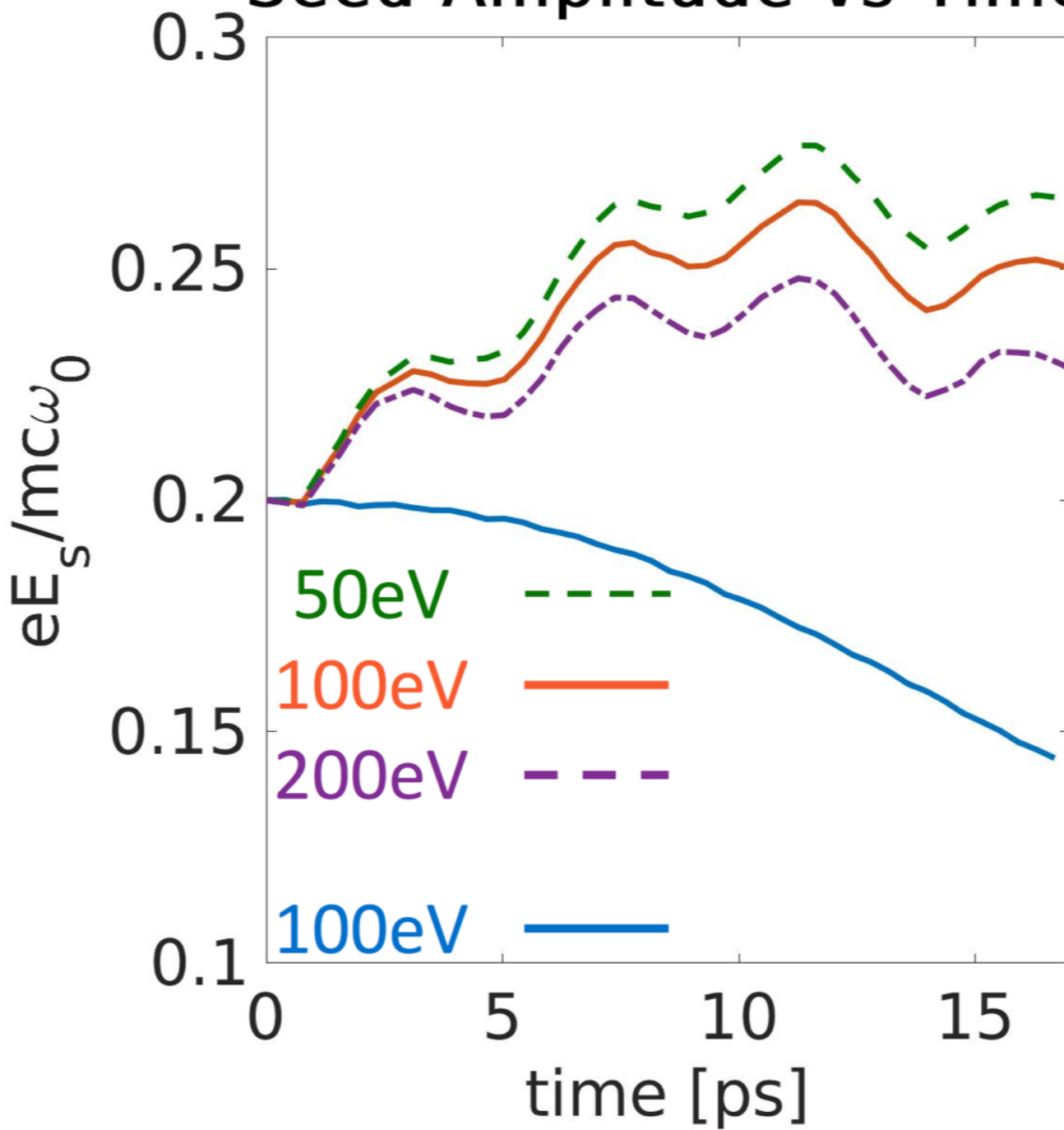




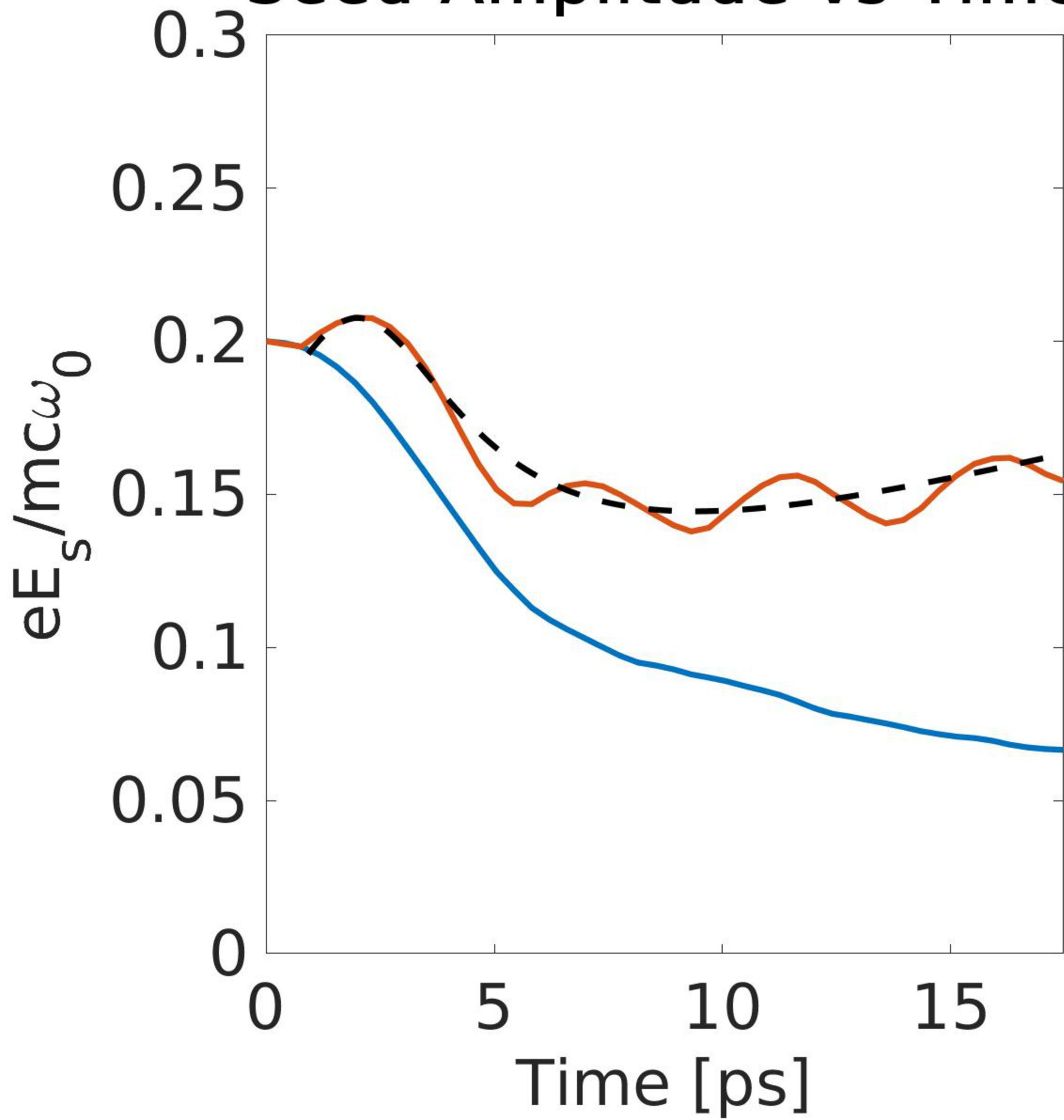




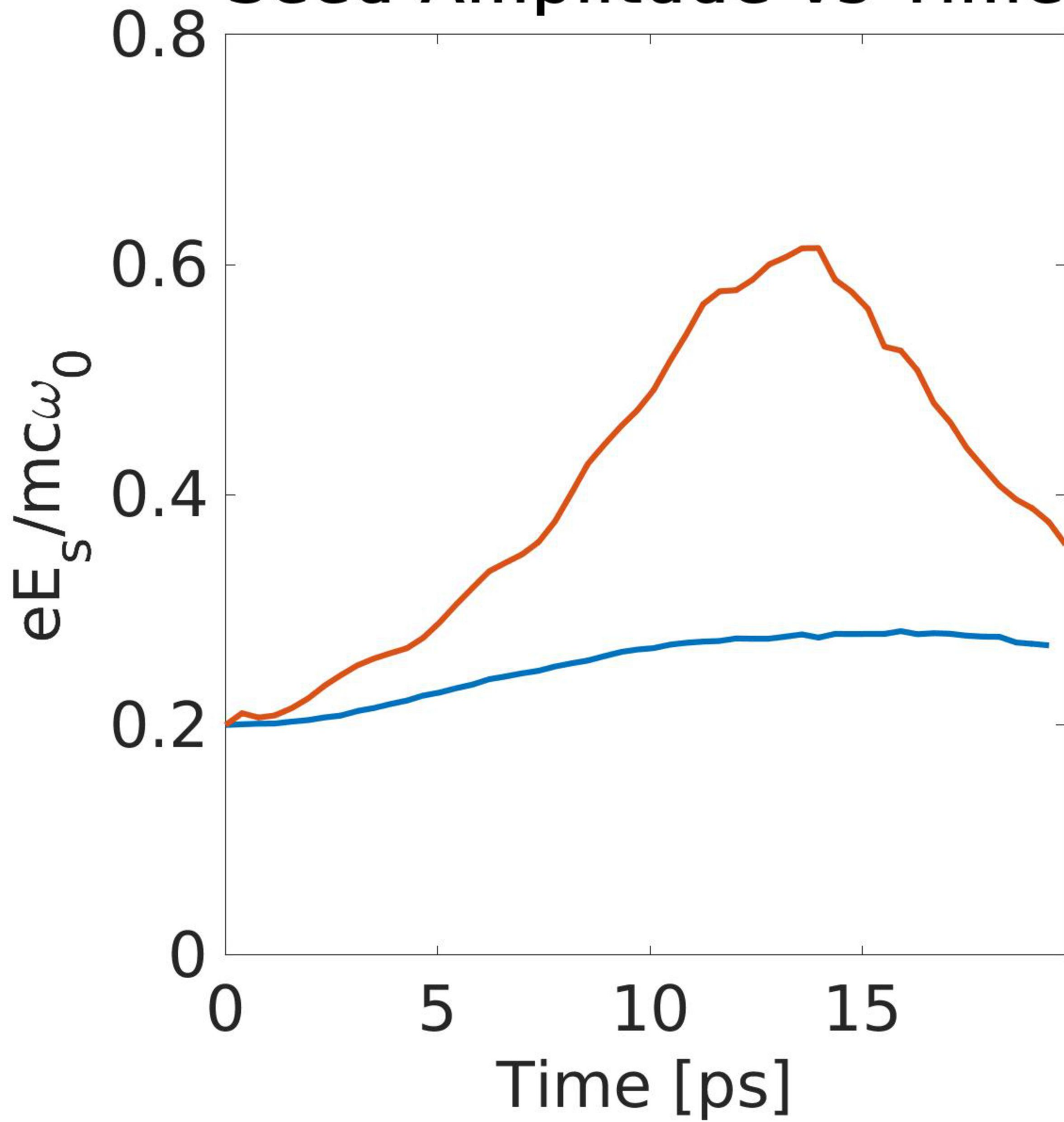
Seed Amplitude vs Time



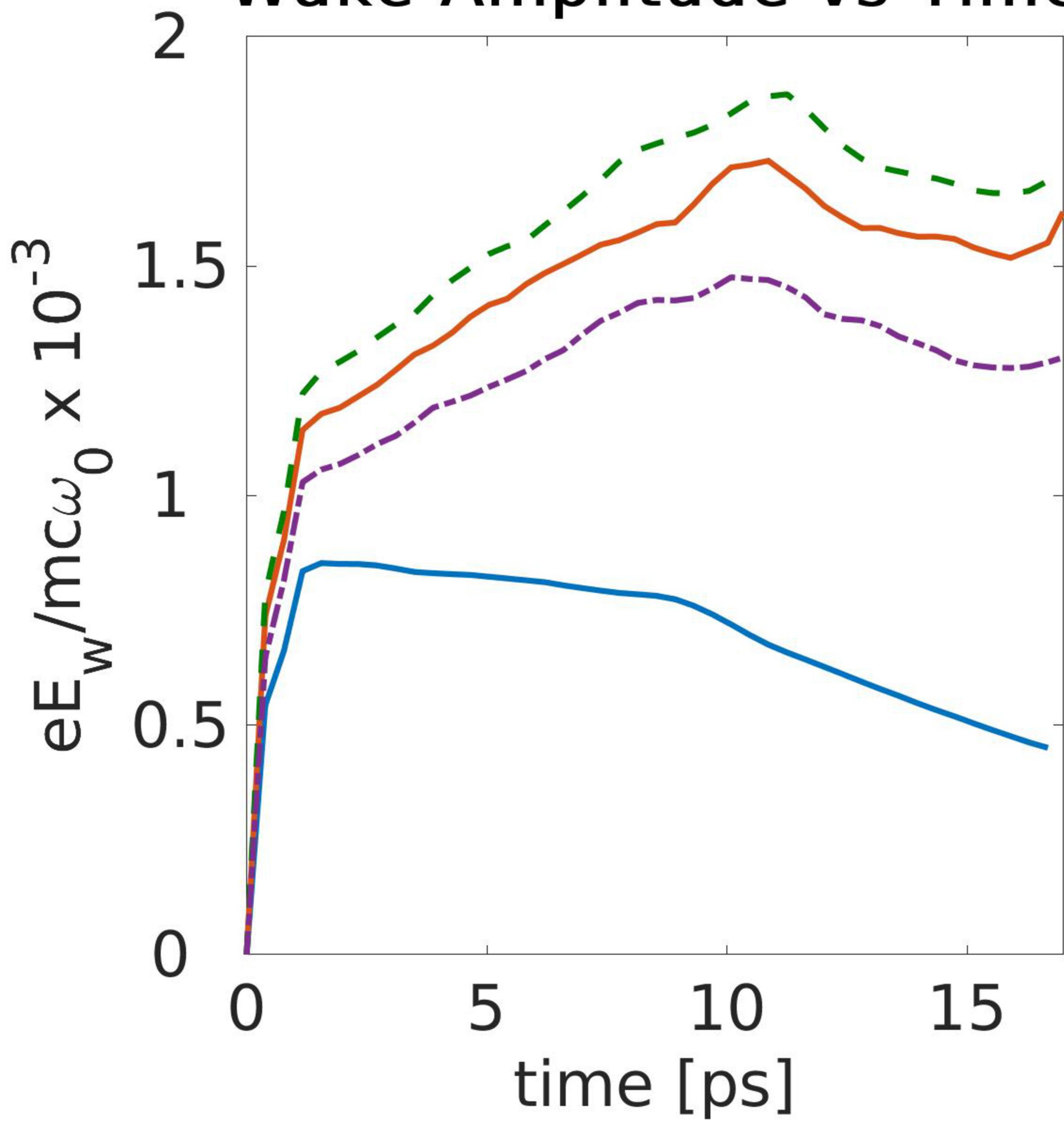
Seed Amplitude vs Time



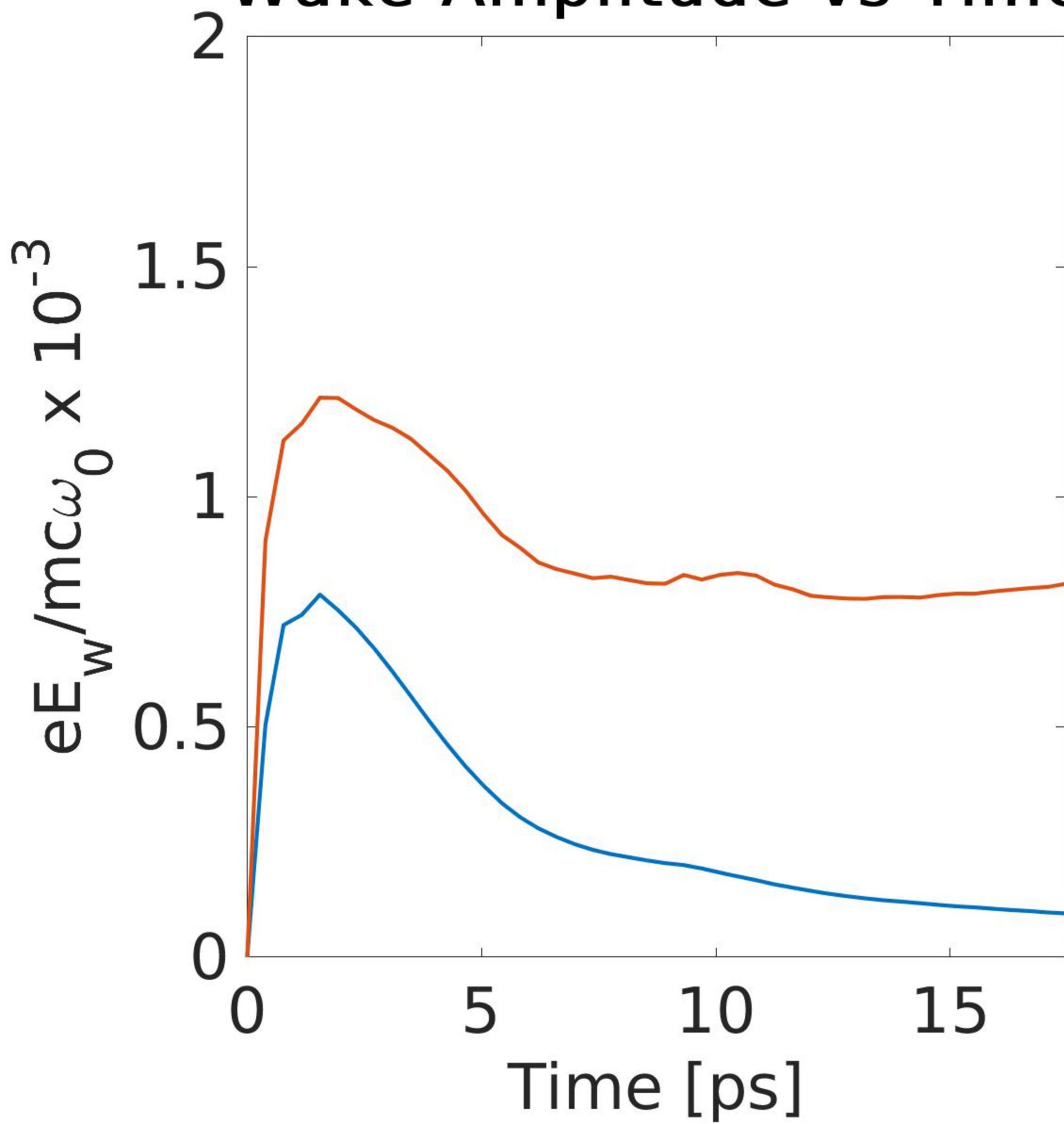
Seed Amplitude vs Time



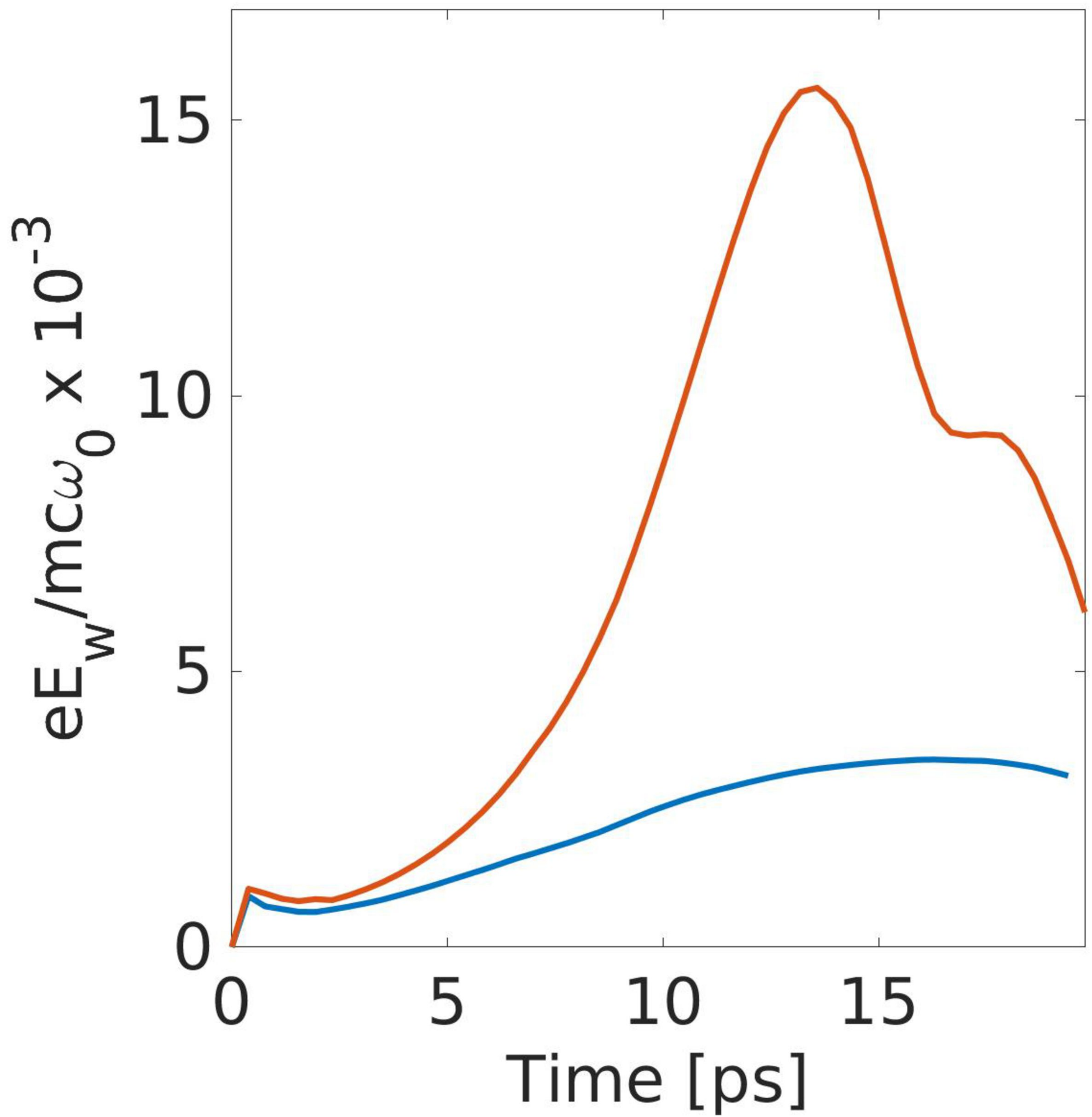
Wake Amplitude vs Time

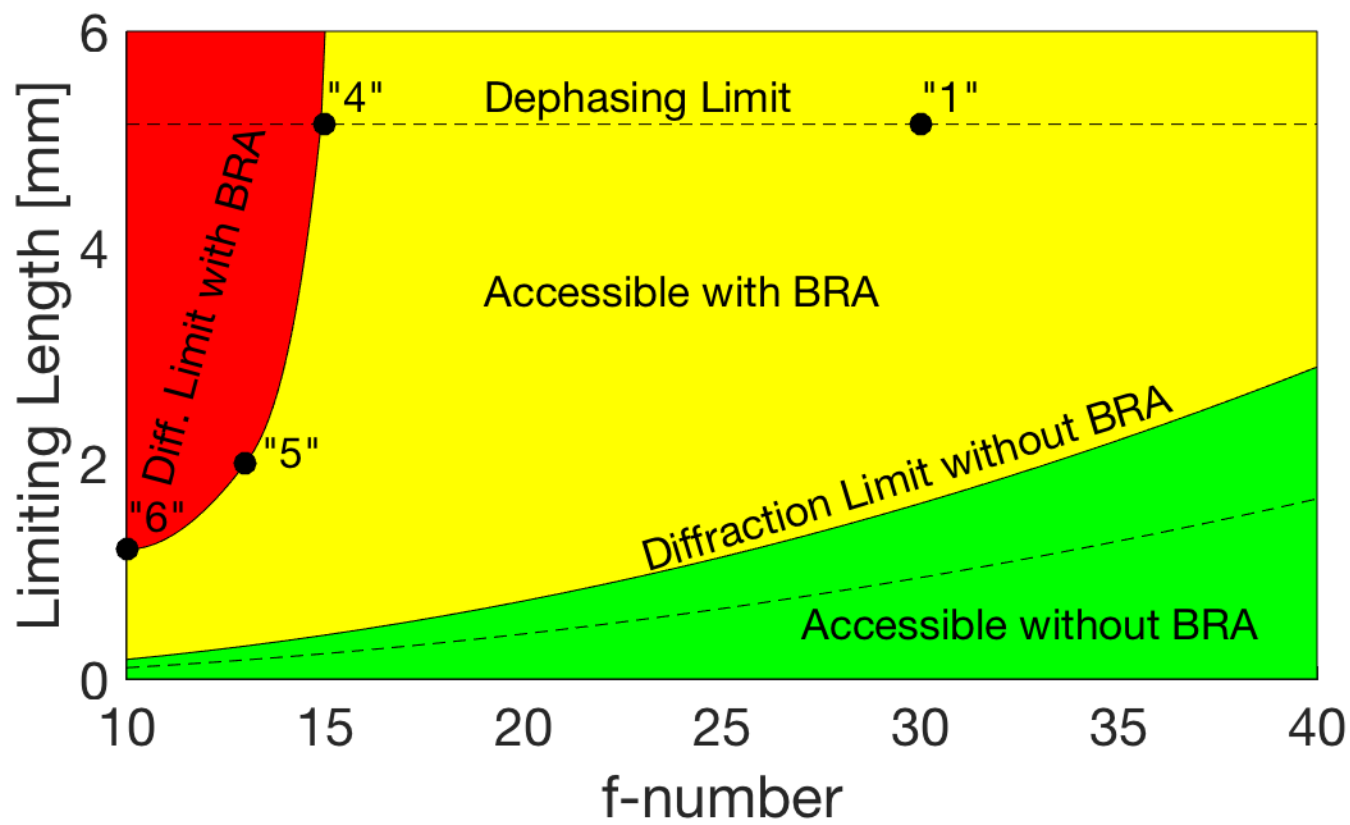


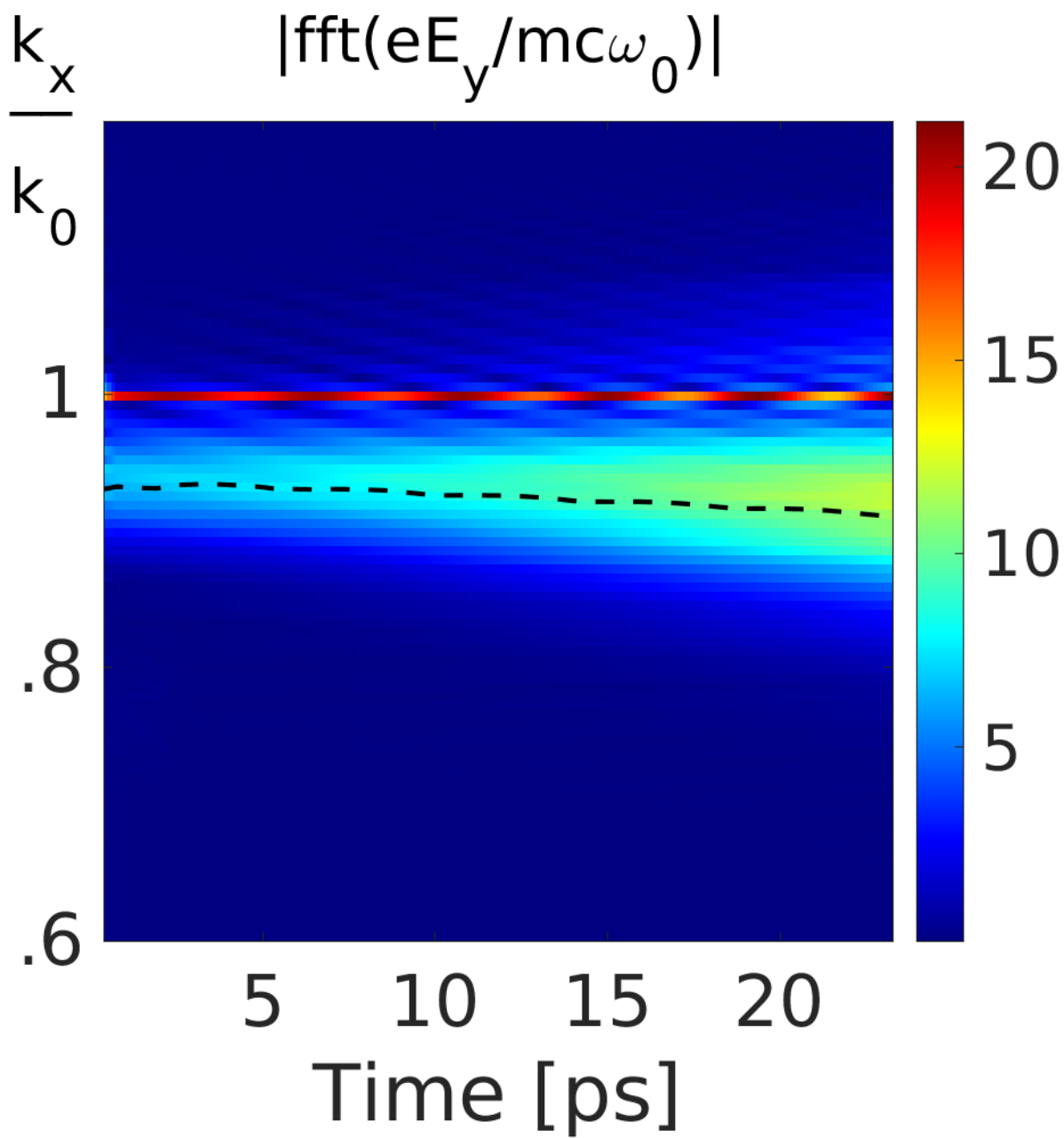
Wake Amplitude vs Time

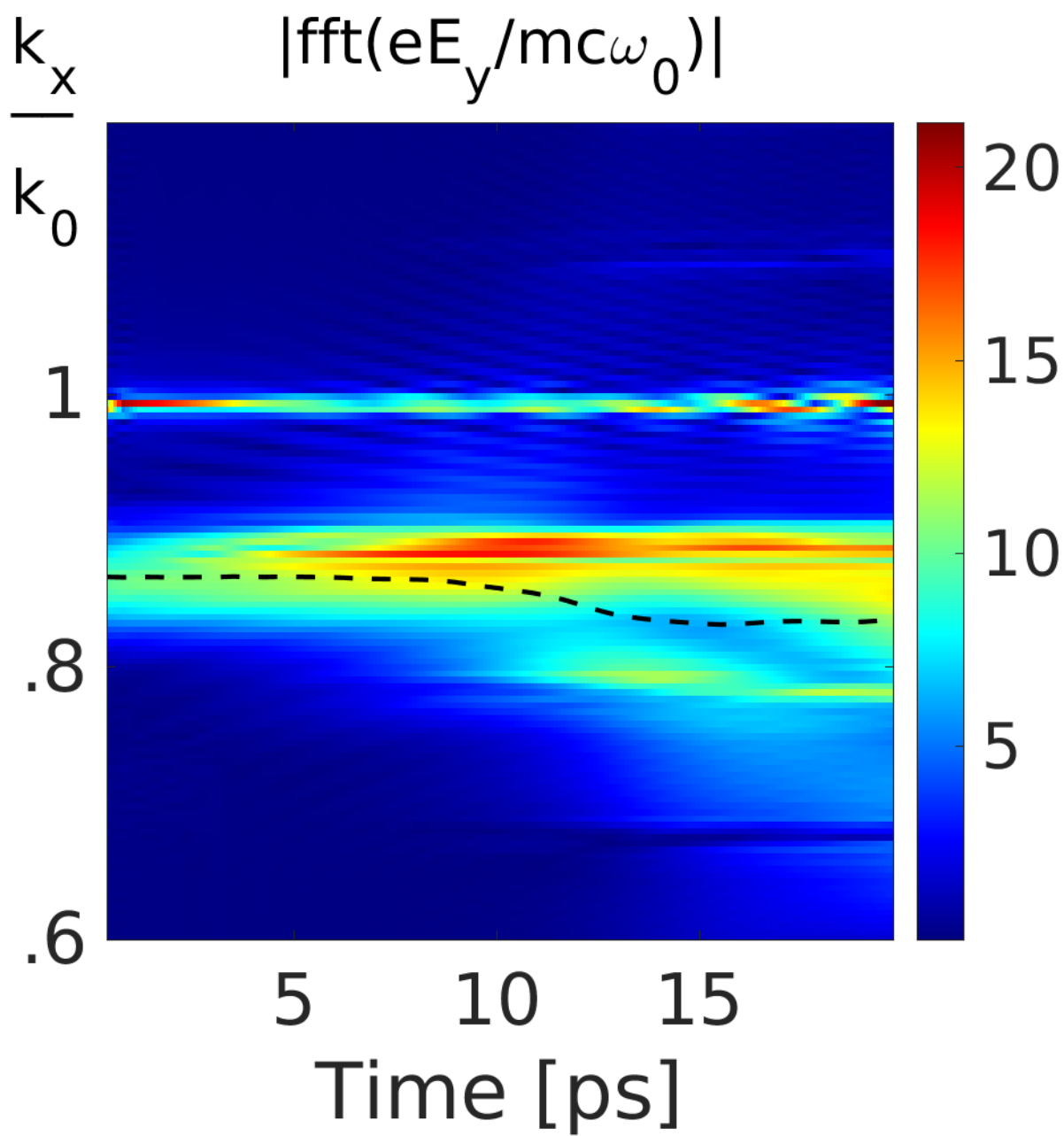


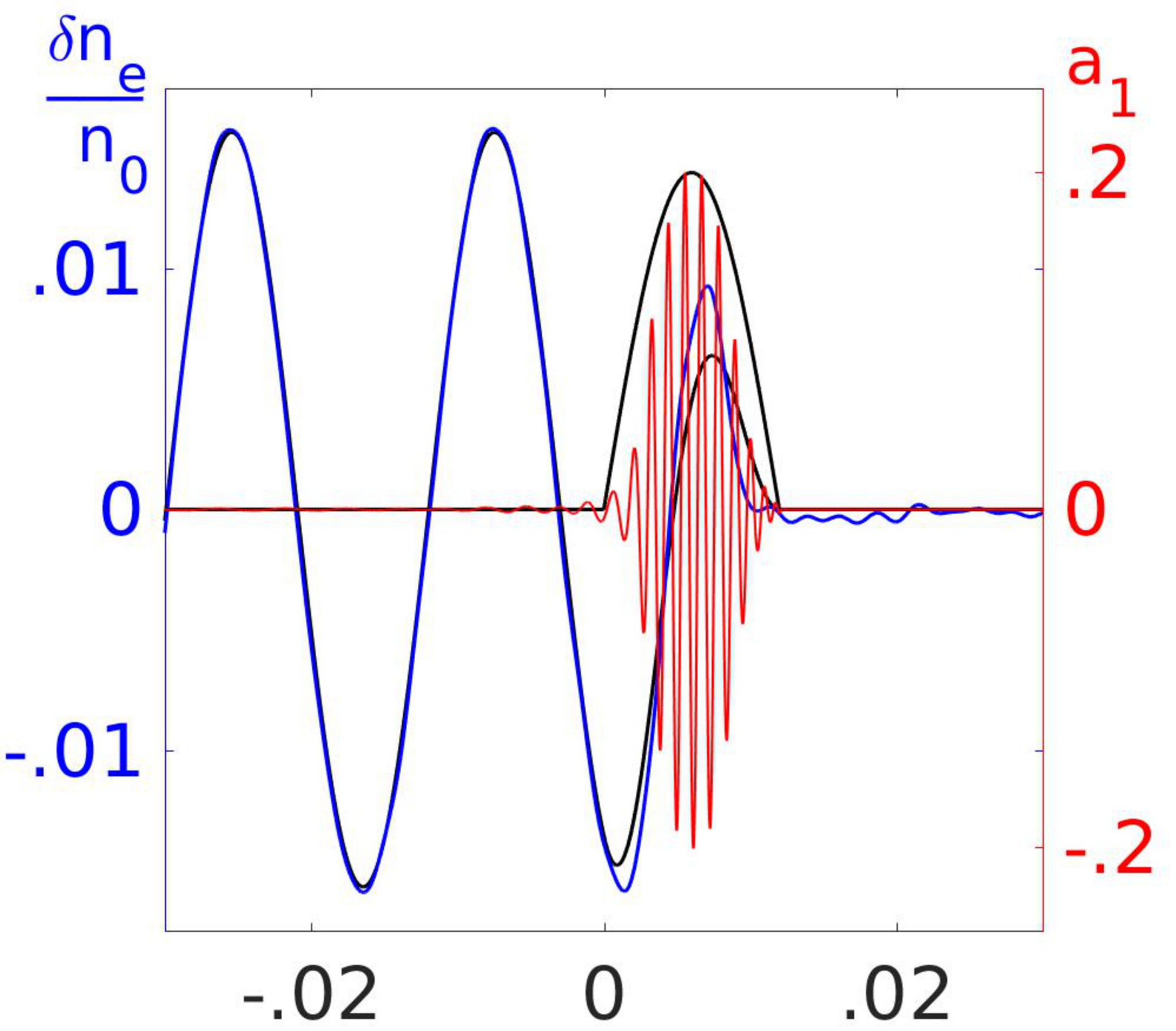
Wake Amplitude vs Time



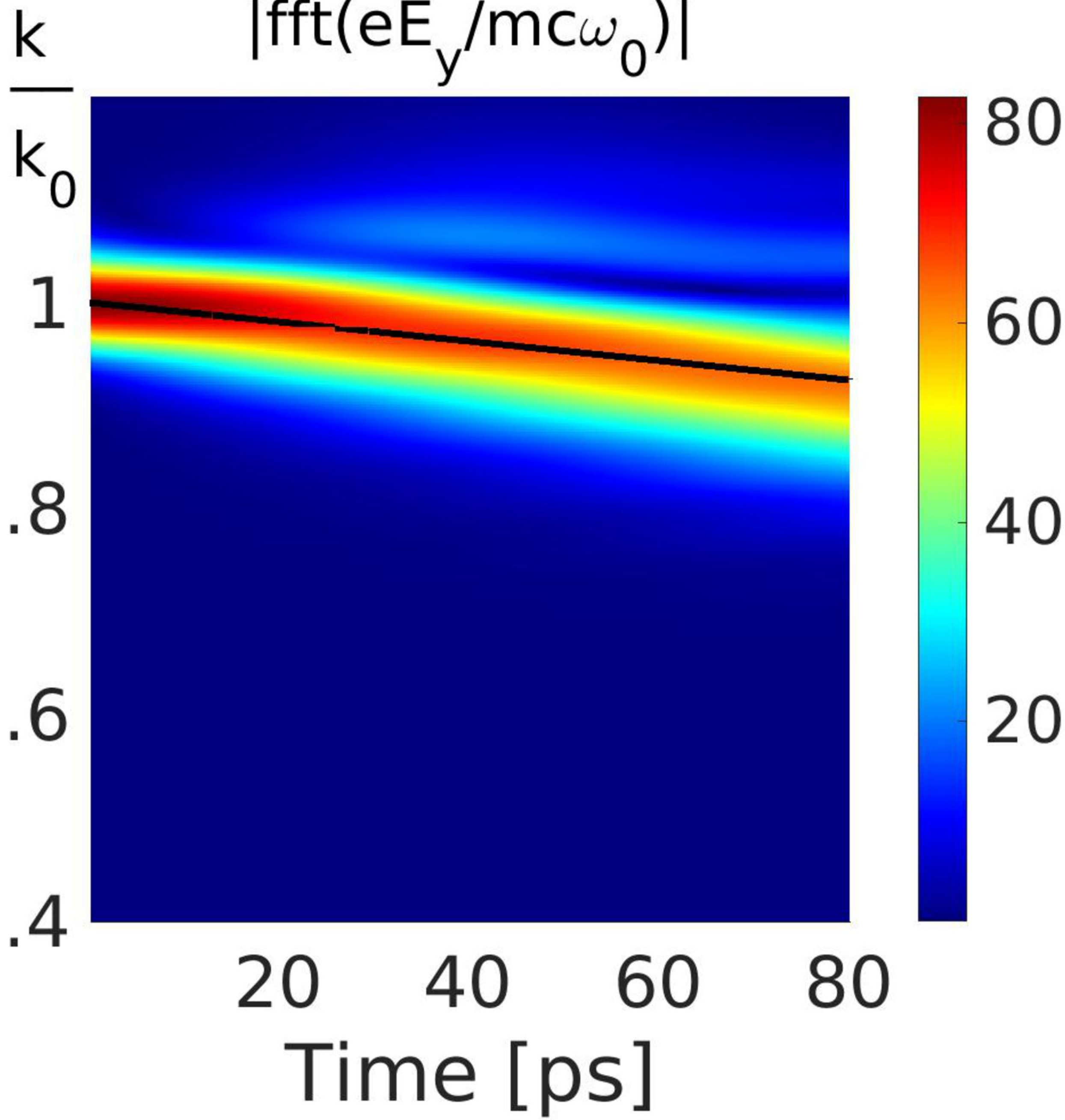


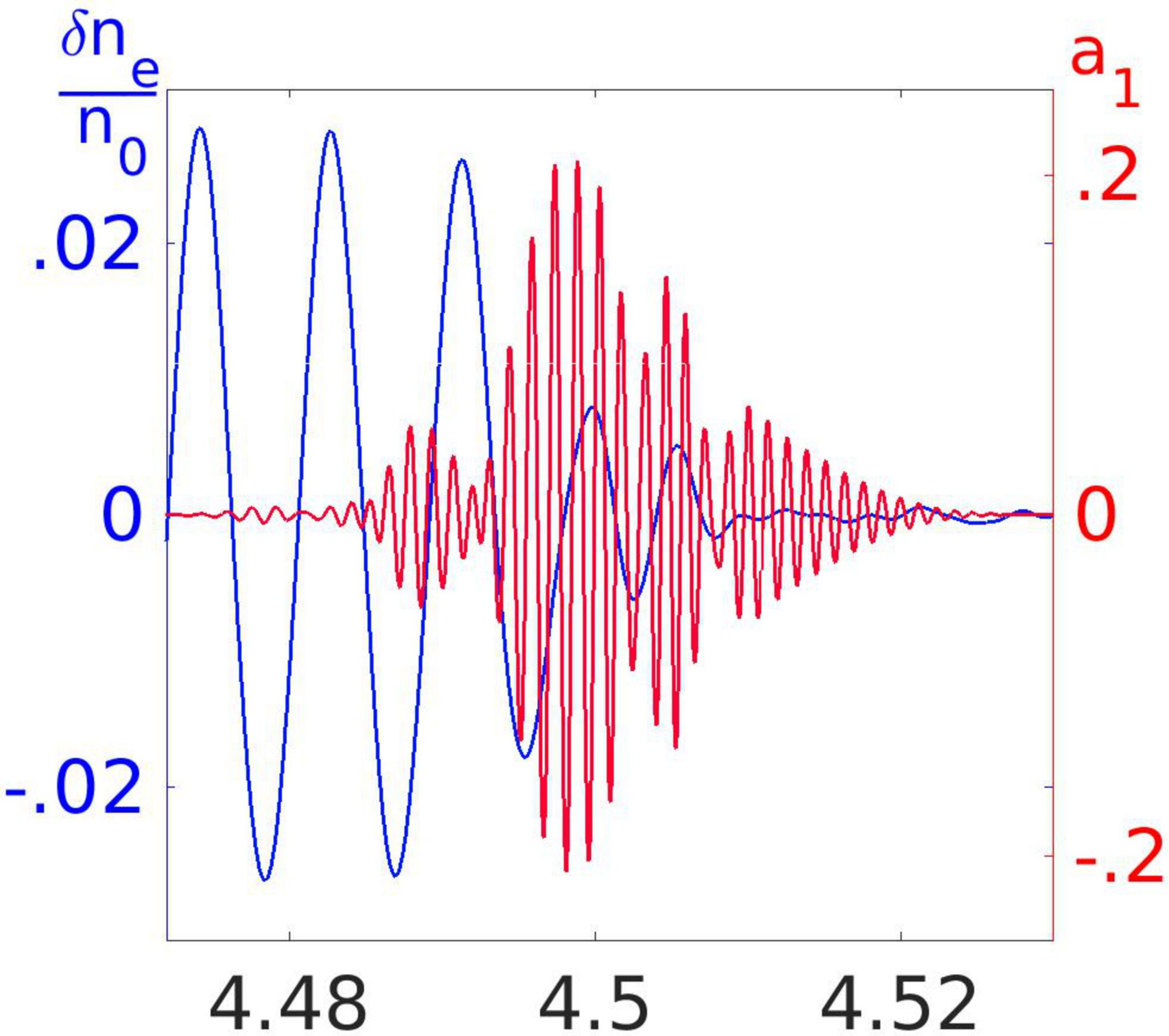




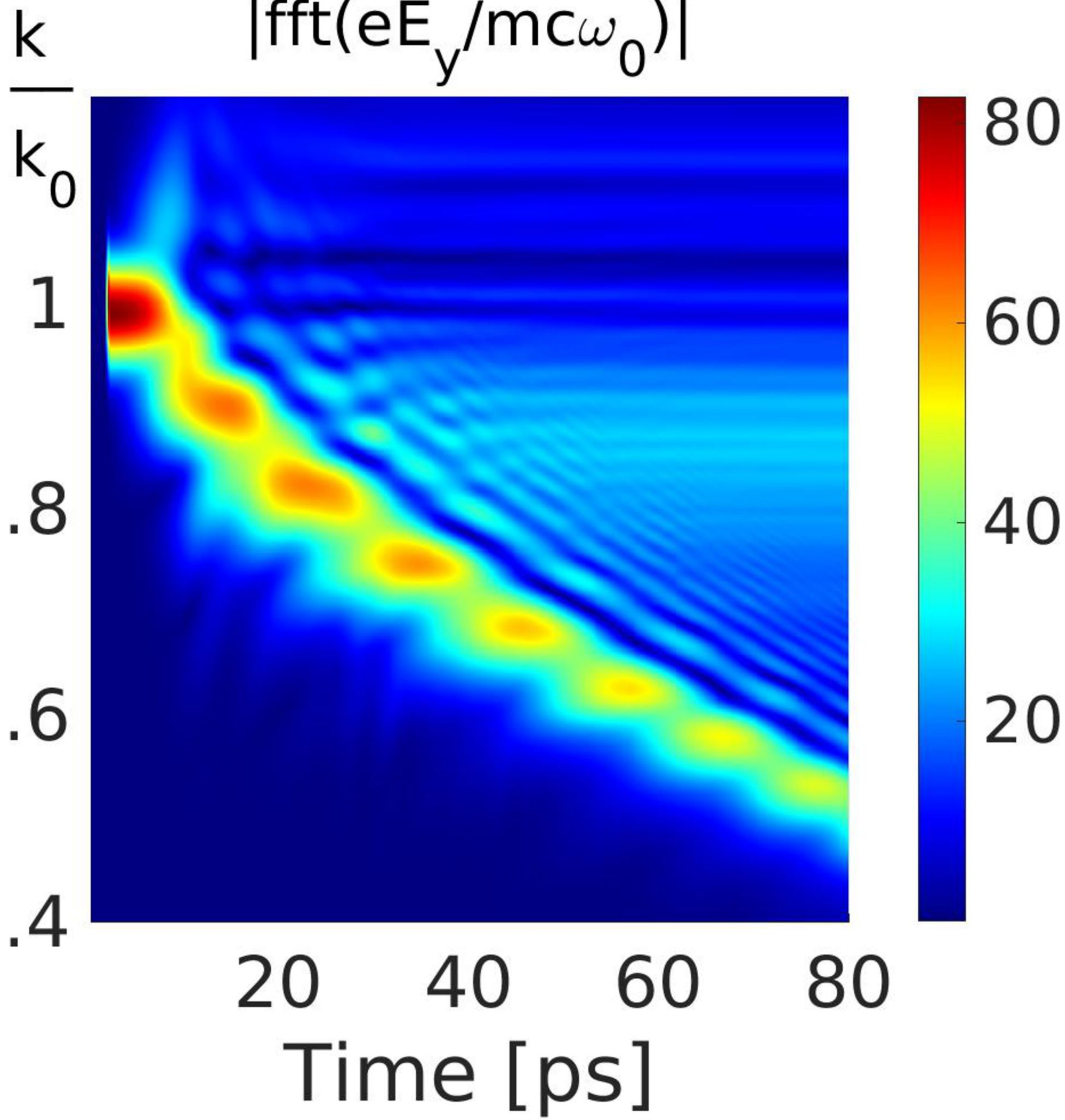


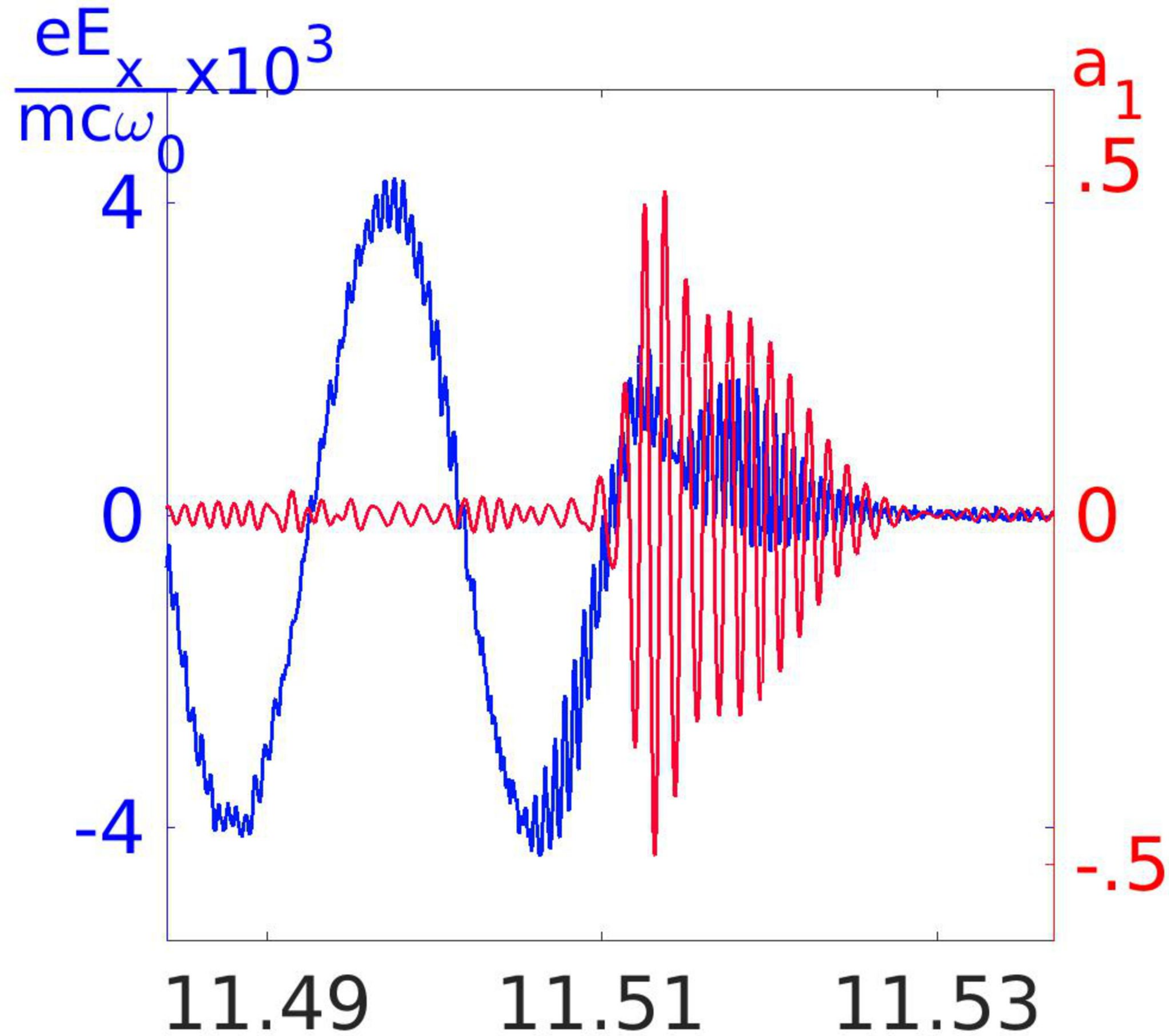
$$|\text{fft}(eE_y/mc\omega_0)|$$



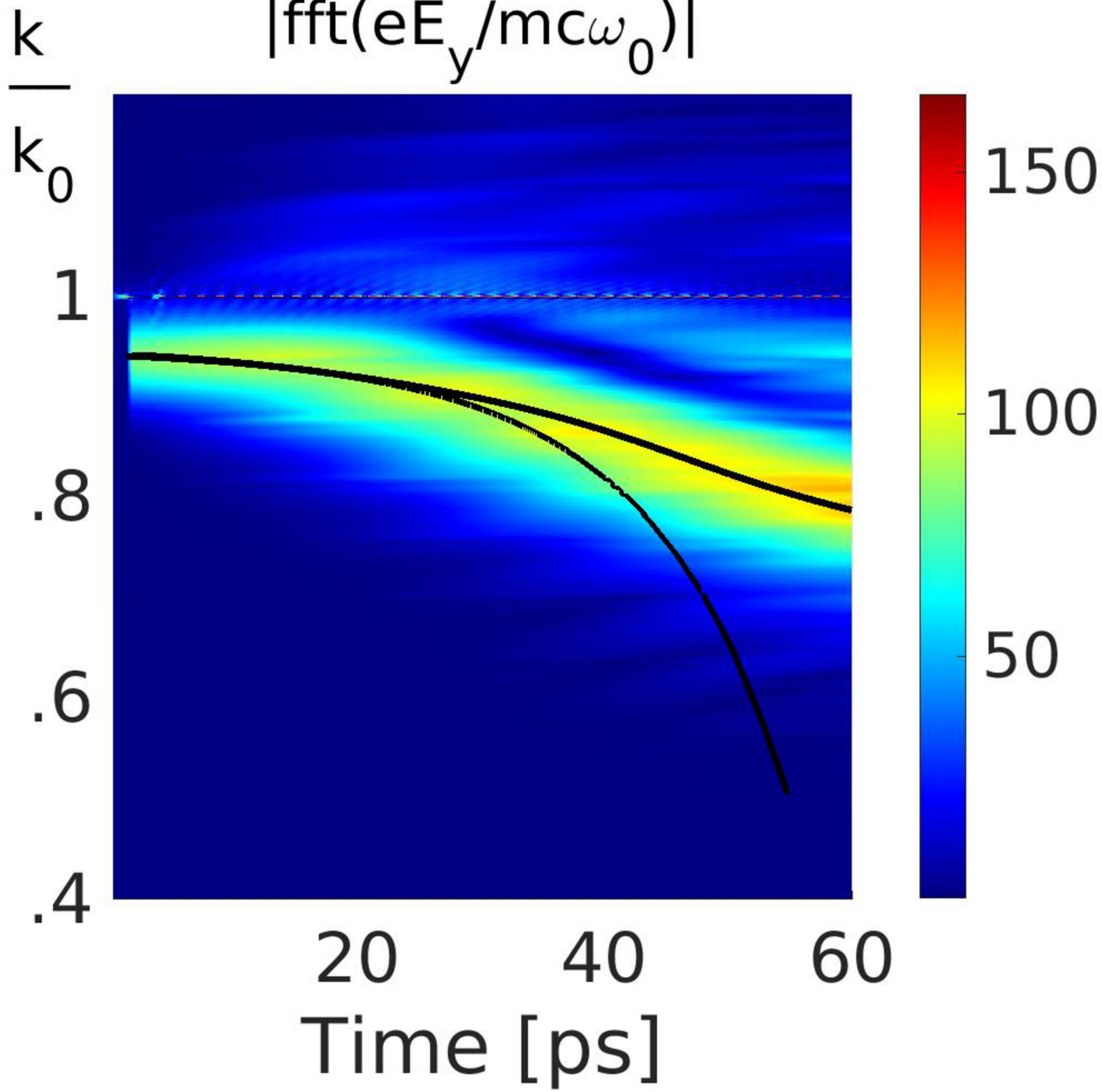


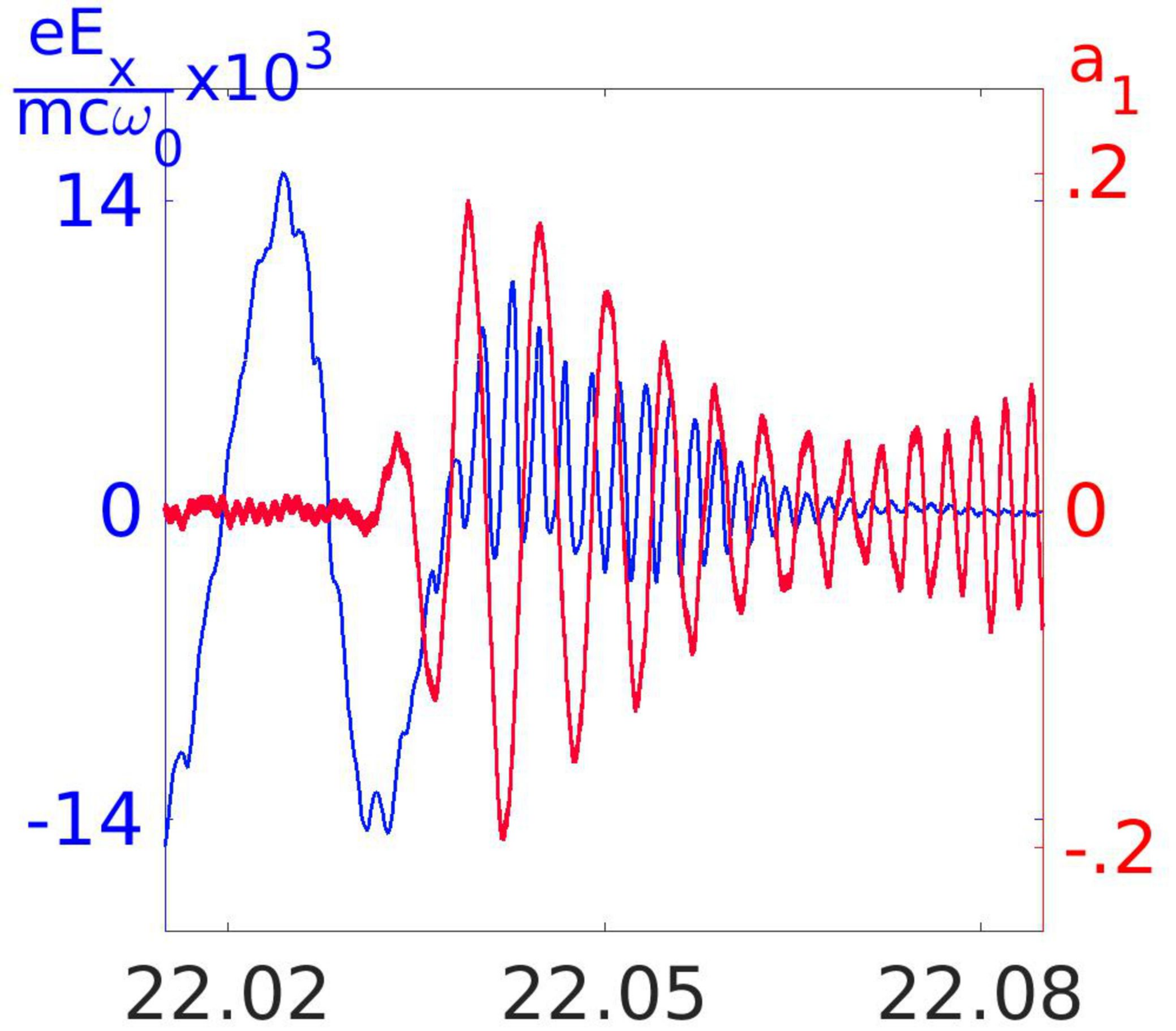
$$|\text{fft}(eE_y/mc\omega_0)|$$



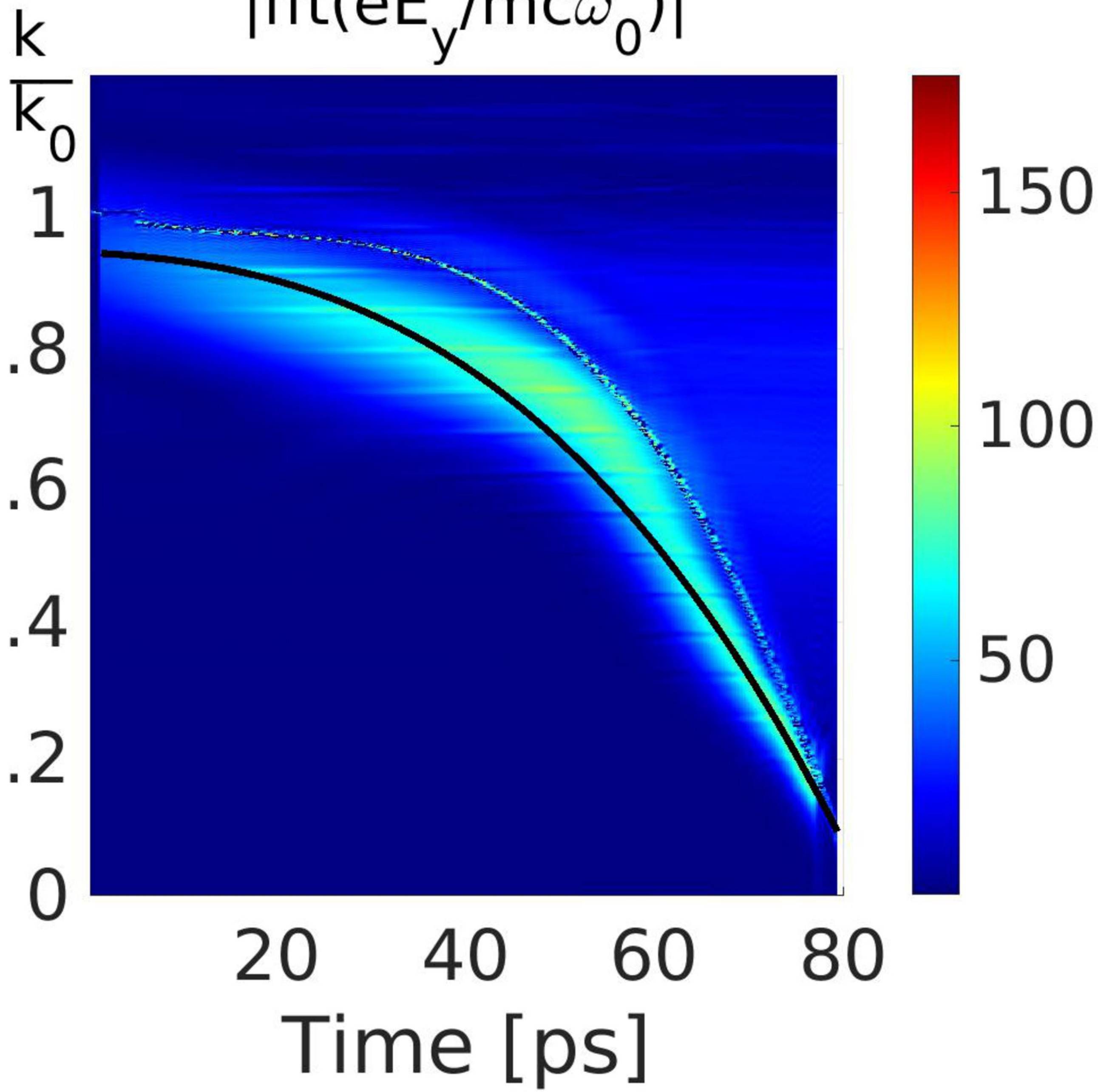


$$|\text{fft}(eE_y/mc\omega_0)|$$

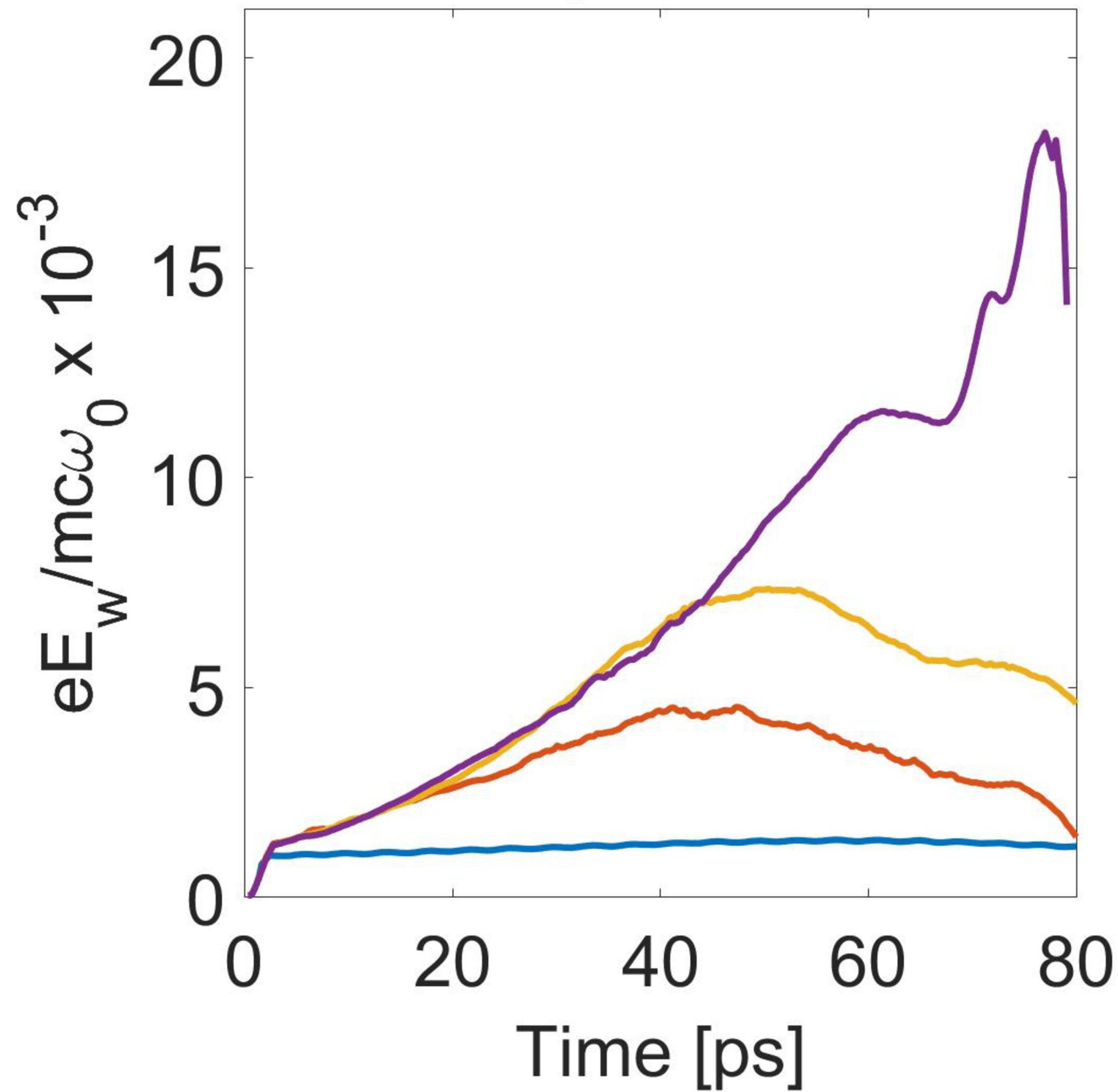




$$|\text{fft}(eE_y/mc\omega_0)|$$



Wake Amplitude vs Time



Wake Amplitude vs Time

